POLITECNICO DI TORINO

Master's Degree in Aerospace Engineering

Master's Degree Thesis

Adaptive Mesh Refinement Driven by Sensors for Hypersonic Flows

Supervisors

Prof. Domenic D'AMBROSIO

Candidate

Simone SASANELLI

July 2024

Summary

Hypersonic is a fascinating area of Fluid Dynamics characterized by strong discontinuities, as shock and expansion waves. Sometimes the irregularities in the flow field can induce to ambiguity and errors in the exact definition of the flow features. In the present work is proposed a new detection method for hypersonic and high-supersonic flow fields which combines the Computational Fluid Dynamics techniques, through the commercial software STAR-CCM+, with the classical detection methods. Starting from well known image processing methods, as Canny-Edge, the core of the work is the creation of sensors able to capture the targeted fluid structures. With this purpose, the model created includes the complementary phases of mesh and sensors creation. The two phases work in parallel due to the fact that the mesh refinement is driven by the detection and the detection success depends on the mesh quality. The aim is to detect the typical hypersonic flow structures as shock and expansion waves, slip lines and wakes to drive the mesh refinement. In particular, the Adaptive Mesh Refinement technique allows to define a dynamic mesh method able to size properly the cells in the target regions. The sensors definition is based on the gradient method, as in the Canny-Edge detection, replacing the brightness intensity with the pressure or the Mach number. However, the gradient condition is not sufficient to obtain accurate solutions. For the detection of shock and expansion waves, a second condition about the Mach normal to the targeted discontinuity is imposed. In fact, a general oblique shock wave could be treated as a normal shock wave superimposed on a uniform flow and the normal direction of the shock wave is perpendicular to the local Mach gradient or pressure gradient. The slip line sensor is based on a double gradient condition, combining a relevant Mach gradient with minimum pressure gradient. As regards the wake, a condition about the total temperature is more appropriate given the large variation in the region where the boundary layer detaches from the body. The final objective of the work is to define normalized functions and present optimum parameters for each sensor. In this way the user can perform the detection of the desired flow feature choosing a value between a specific range obtained by the simulations executed and refine consequently the grid.

Acknowledgements

I would like to express gratitude to my supervisor Professor Domenic D'Ambrosio for his invaluable support and constant guidance throughout the entirety of the work. His passion for Aerodynamics and Computational Fluid Dynamics pushed me to deeply commit to the project. I am grateful for the knowledge matured during this journey thanks to his experience.

I would like to extend my eternal gratitude to my family. Thank you for your endless love and the precious support, essential to achieve such a great result. Thank you for inspiring me and for being the model I aspire to every day. I will be always grateful to you for the experience you allowed me to do.

I am deeply grateful to my friends and the people close to me in the last two years. Thank you for the invaluable time spent together and the positive influence you bring to my life. Without you this would not be possible.

Lastly, I am proud of the personal and academic growth I gained during the entire experience. I am proud of the dedication, the effort and the attitude I put every single day. All the moments have marked strongly my personality and allowed me to face life with a different approach.

Explore Dream Discover

Table of Contents

List of Tables

List of Figures

Chapter 1

Introduction

Hypersonic flows are characterized by distinctive features such as shock waves, contact surfaces, strong expansions, thick boundary layers, and bulky wakes due to the geometric bluntness typical of vehicles operating in this regime [1].
In Computational Fluid Dynamics (CFD) simulations, capturing these details with sufficient accuracy is a significant challenge because their exact positions are not known a priori, making it impossible to generate an adequate mesh before one or more simulations have been carried out. Additionally, structured grids are not well-suited for this task as they are inefficient when local refinement is required in specific flow regions. Therefore, adaptive mesh refinement is the best choice for resolving localized flow characteristics.
This work aims to define effective detection methods based on CFD results combined with sensors and/or with image processing techniques, such as the Canny Edge method [2]. The latter is a useful tool for refining the CFD mesh by creating sensors capable of capturing the desired flow features. The work carried out in the thesis is described in this manuscript as follows.
The second chapter describes the typical hypersonic flow features. Hypersonic flows are characterized by interactions not only between the fluid and the vehicle but also among fluid features, such as shock-shock and shock-boundary layer interactions. The governing equations and relations of typical hypersonic features are detailed in this chapter.
The third chapter provides an analysis of the scientific literature on sensors and filters for supersonic and hypersonic flows [3], with an overview of the Canny Edge detection process. It also introduces the Adaptive Mesh Refinement method and the case studies considered. Specifically, simulations are conducted on inviscid and viscous cases using the commercial software STAR-CCM+.
The fourth chapter covers the first operational part of the work. After an overview of the mesh properties, the Adaptive Mesh Refinement method is explained in detail, along with the analysis conducted to obtain the final formulation of the

refinement function. The goal is to drive the refinement through hypersonic sensors. This chapter also details the physical relations used to define the sensors and the filters proposed for the detection.
The fifth chapter describes the settings related to the simulations in STAR-CCM+. It explains the functions used for each case study and the parameters involved in the detection. The purpose is to conduct a sensitivity analysis to determine the optimum values for each sensor.
The sixth chapter presents the results through the sensor contours from the detection process. Each case study result is shown with plots related to the sensors and the mesh refinement function. The chapter also discusses the optimum parameters used for the final simulations where convergence is achieved.
The final chapter provides a brief overview of the work, introducing the conclusions and objectives achieved. A comparison with the theoretical results for each case study is provided to conclude the work. Future improvements are also discussed in this chapter.

Chapter 2

Hypersonic Flows

2.1 Hypersonic Interactions

In this section is proposed the theory related to the flow interactions explained with some practical examples. Considering a flat plate in a hypersonic flow, the boundary layer represents a virtual obstacle for the impinging flow. Its shape is described by the displacement thickness, therefore the incoming flow will be deflected given the presence of the boundary layer generated by the no-slip condition to the wall. An oblique shock wave is thus produced and modifies the flow properties outside the boundary layer with respect to the freestream. Also the boundary layer is affected by the shock wave generating a mutual interaction between the outer inviscid flow and the boundary layer [1]. This is a typical example of hypersonic viscous interaction.

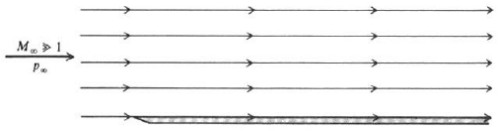

Figure 2.1: Inviscid Interaction

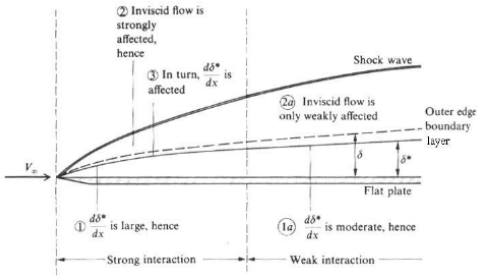

Figure 2.2: Viscous Interaction

In the inviscid case, the flat plate presence does not perturbe the incoming flow field; in the viscous case, the flow deflects due to the presence of the boundary layer which modifies and increases the shape of the body.

2.1.1 Pressure Interaction

The pressure interaction occurs when the wall pressure distribution is larger than the freestream pressure close to the leading edge and tends to decrease moving downstream, until the value of freestream is reached. Moreover, the region close to the leading edge where the shock layer and the boundary layer are indistinguishable is called Merged Layer. Moving downstream the boundary and the shock layer become separate entities as the decrease of the mutual interaction. The hypersonic viscous interactions are governed by the following parameter [1]:

$$\overline{\chi} = \frac{M_{inf}^3}{\sqrt{Re_{x,inf}}}\sqrt{C} \tag{2.1}$$

With:

$$C = \frac{\rho_w \mu_w}{\rho_e \mu_e} \tag{2.2}$$

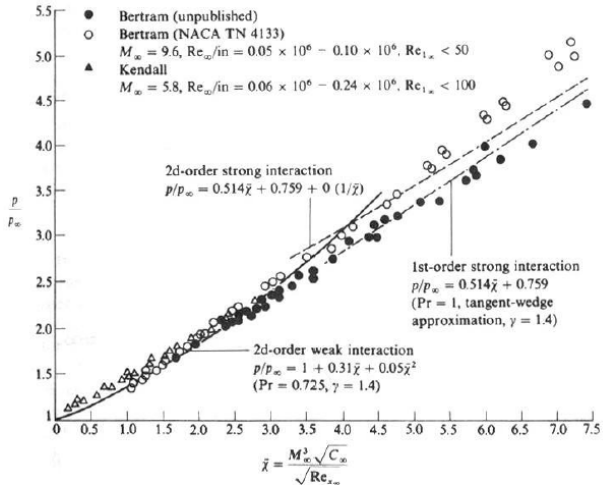

Figure 2.3: Chi-bar

In particular, for practical purposes:

- Strong Interaction: $\overline{\chi} > 3$
- Weak Interaction: $\overline{\chi} < 3$

2.1.2 Shock - Shock Interaction

A viscous interaction related to the shock waves occurs when a shock wave intersects with another shock wave. This phenomenon is called shock - shock interaction.

These interactions can produce localized heat loads and can be present in different part of the vehicle as at wings or stabilizers, at a control surface or ahead of a canopy, at the cowl lip of an inlet, in the internal part of an inlet [1].

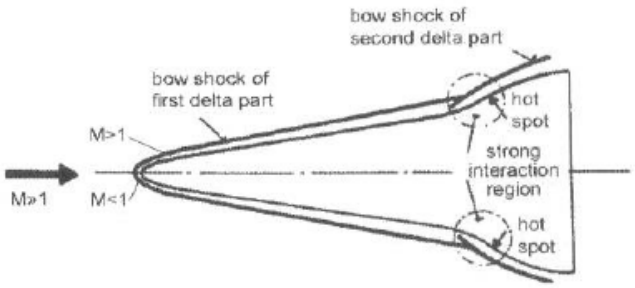

Figure 2.4: Bow Shocks Interaction

In Fig.2.4 is proposed a strong interaction of the first bow shock with a second bow shock at a second delta part of the wing of a CAV-type vehicle [1].

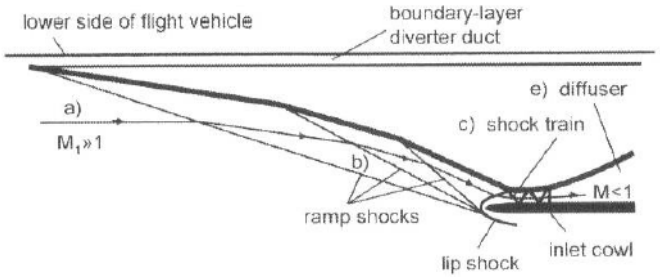

Figure 2.5: Shocks Interaction and Shock Train

In the figure is shown a three-ramp ramjet engine inlet with the interaction between shocks of the same family which produce a coalescent shock given their interaction. A bow shock is generated at the impact with the lip. Moreover, a shock train can enter in the inlet cowl and can exceed the stress limit of the structures.

Shock Waves Interaction of Same Family

A typical hypersonic phenomenon occurs when compression wave of the same family intersect generating an oblique shock wave. Moreover, when shocks of the same family intersect, from the intersection point another wave is generated. This could be an expansion or compression wave according to the intensity of the shocks [4]. A slip line separates regions with same pressure and velocity direction, but different entropy and magnitude velocity due to the fact that the two flows move across

different shock waves. The entropy discontinuity is larger across a single shock with respect to the transition through a multiple shock.

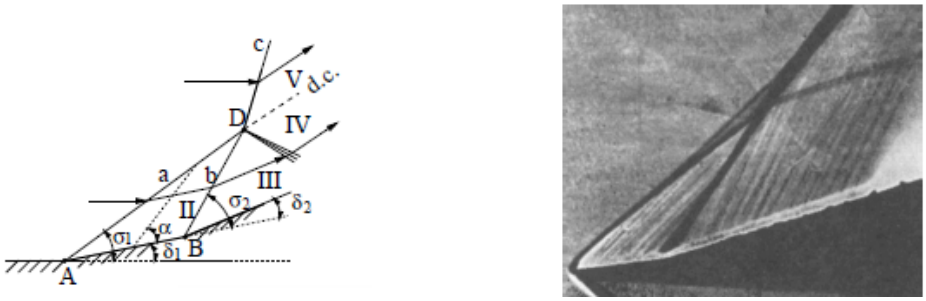

Figure 2.6: Shocks Interaction of Same Family

Shock Waves Interaction of Opposite Family

Another typical hypersonic phenomenon occurs with the interaction of shocks of the opposite family generated by two different deflections of the superior and inferior wall of a duct. The same interaction type occurs also at the outlet of an overexpanded nozzle. The shocks are produced to respect the condition on the pressure at the edge of the jet which must be equal to the external pressure. In this case, given the same intensity of the shocks, no slip lines are generated and a shocks reflection phenomenon is caused [4].

Figure 2.7: Shocks Interaction of Opposite Family - Overexpanded Nozzle

2.1.3 Shock - Boundary Layer Interaction

A viscous interaction related to the shock waves occurs when a shock wave impinges on the boundary layer. This phenomenon is called shock - boundary layer interaction and is critical for vehicle in hypersonic flows. In general, shock wave - boundary layer interactions are classified as Edney-Type Interactions. Here are proposed two typical examples, the ramp-type interaction or Edney type V- VI and the nose/leading-edge-type interaction or Edney type III- IV [1].

Laminar and Turbulent Boundary Layer Interaction

This interaction is complex and depends on the nature of the boundary layer. Considering a laminar case, if an oblique shock wave impacts on the boundary layer, it curves and weakens progressively until the sonic line. Given the thickening of the boundary layer, in the supersonic region of the boundary layer are generated compression waves which intersect producing an oblique shock wave. Moreover, when the impinging shock penetrates the boundary layer, an expansion fan is generated and the flow is deflected again. A second compression wave is caused by the concavity of the boundary layer where the flow reattaches after the deflection of the expansion. These compression waves are coalescent in another oblique shock wave. In conclusion, a reflection system is developed and is composed by two coalescent shocks upstream and downstream the impact point and an expansion wave. A turbulent boundary layer, given the more intense momentum fluctuations, is less sensible at the adverse pressure gradient [4]. The shock effect are less intense and the region of the boundary layer influenced by the shock is smaller.

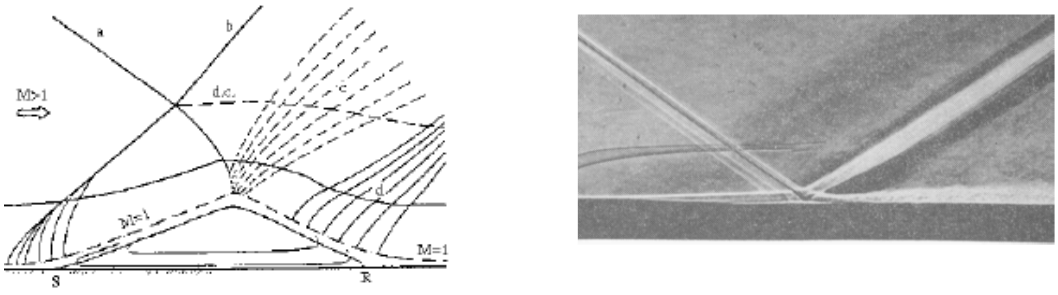

Figure 2.8: Shock - Boundary Layer Interaction

Ramp Interaction - Edney V - VI

Considering a hollow cylinder/extended flare configuration, the interaction occurs when the shock wave generated by the ramp interacts with the boundary layer. The strong adverse pressure gradient caused by the presence of the wedge generates the separation of the boundary layer. The interaction phenomenon is complex and multiple shocks are generated. A first shock is produced by the impact of the freestream with the corner; a second shock is caused by the impact with the separation bubble; a third outer shock and a fourth stronger inner shock are produced by the reattachment of the flow to the wall; a fifth coalescent shock is generated at the triple point given the intersection of the first, second and third shock waves [1].

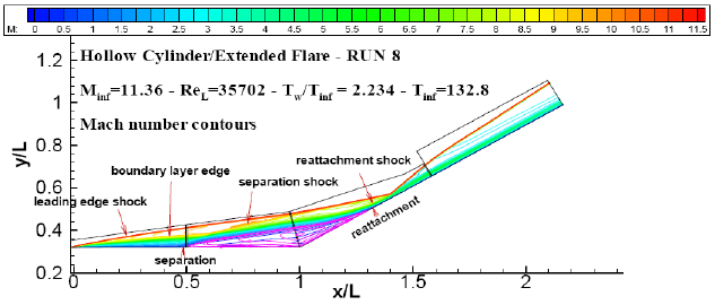

Figure 2.9: Shock Waves - Mach Number Contours

Moreover, the intersection point causes the development of an expansion fan and a slip line. In this region are present high values of pressure and heat flux.

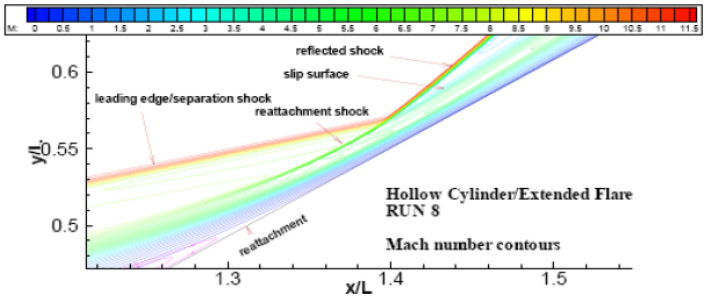

Figure 2.10: Expansion Fan and Slip Line - Mach Number

Nose-Leading Edge Type Interaction - Edney III - IV

Nose/leading edge interactions are critical for cowl lips and unswept pylons as they lead to localized regions of surface pressure and heat transfer rates on the body [1]. The Edney type IV is the most severe with respect to the III. Edney type interactions occur when an oblique shock wave intersects with a detached shock that forms ahead of a blunt body. Various shock interference patterns can occur when the impinging shock interaction with the bow shock is strong, that is between the upper and lower sonic lines. The two interfering shocks have different intensities and a shear layer separates region with subsonic flow from region with supersonic flow. According to the angle of impact between the shock and the shear layer, it is possible that the shear layer reattaches on the obstacle. This corresponds to a type III interference [1].

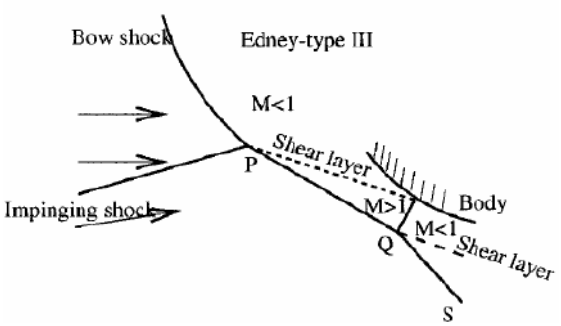

Figure 2.11: Type III Interference

When the inclination is too large a supersonic jet is formed, and if it is directed toward the body the flow undergoes strong compression across a normal shock [1]. This is called type IV interference and generates the highest values of pressure and heat transfer on the body surface.

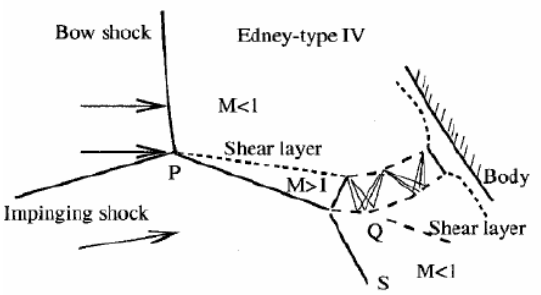

Figure 2.12: Type IV Interference

2.2 Physics Continuum

In this section is proposed the physics of the simulations executed in STAR-CCM+. The model is set to run two dimensional and steady state equations. This choice allows to remove the time dependency, thus the equations integration occurs only in space and not in time. No temporal scheme are imposed. The inviscid cases are modelled according to the ideal fluid approximation which allows to neglect the terms related to the shear stresses and heat transfer if the Reynolds number is sufficiently large [5]. The governing equations for an ideal fluid are called Euler equations. The viscous cases are modelled with the classical Navier Stokes equations which includes all the terms related to the effects of viscosity and heat transfer. The turbulence is set with the Laminar model.

2.3 Typical Hypersonic Flow Features

In hypersonic flow fields, the freestream undergoes strong compression effects. Energy dissipation or high temperatures phenomena are necessary to deflect the flow and respect the tangency condition to the wall. The classical hypersonic fluid structures are shock and expansion waves, bow shock in the case of blunt body geometries, contact surfaces and interactions between all these characteristics.

2.3.1 Shock Waves

High speed flows are characterized by strong compression that occur in a very short distance, i.e. shock waves. These are treated as discontinuities in the flow field given the increase in terms of pressure, temperature, density and entropy, and the decrease in velocity and total pressure. The shock waves are classified in normal shock waves, when the streamlines cross the shock flow in a direction perpendicular to the shock itself, and oblique shock waves when the shock is deflected with an angle with respect to the incoming flow [5]. As mentioned in the introduction, the detection method applied in the work is based on a combination between the Canny-Edge and the classical Rankine-Hugoniot equations for shocks. In the following subsections are briefly proposed the shock's relation for both the cases and at the end are presented the jump relations variation for freestream Mach tending to infinite with a mention to the Oswatitsch Independence Principle.

Normal Shock Wave

The flow across the normal shock wave undergoes a strong compression so that the flow becomes subsonic from supersonic. The assumption considered for the shock wave are: steady and adiabatic flow, no viscous effects because the flow is uniform upstream and downstream the shock wave and no body forces. Under these hypothesis, the Navier Stokes equations become:

$$\int_S \rho \mathbf{v} \cdot \mathbf{n} dS = 0 \tag{2.3}$$

$$\int_S \rho \mathbf{v}\mathbf{v} \cdot \mathbf{n} dS + \int_S p \cdot \bar{\mathbf{I}} \cdot \mathbf{n} dS = 0 \tag{2.4}$$

$$\int_S (E + p)\mathbf{v} \cdot \mathbf{n} dS = 0 \tag{2.5}$$

With the assumptions considered, managing the Navier Stokes equations it is possible to obtain the fundamental normal shock relations:

$$\rho_2 u_2 = \rho_1 u_1 \tag{2.6}$$

$$p_2 + \rho_2 u_2^2 = p_1 + \rho_1 u_1^2 \tag{2.7}$$

$$h_2 + \frac{1}{2}u_2^2 = h_1 + \frac{1}{2}u_1^2 \tag{2.8}$$

The last equation states that the total enthalpy remains constant across a normal shock wave. In fact, this is an important result according to also the total temperature remains constant across the normal shock. The total pressure, since the entropy grows, must decrease across the shock. The jump relations across the normal shock wave, or Rankine-Hugoniot equations, describe the discontinuity of the flow quantities from the upstream to the downstream condition. In particular, this phenomenon is characterized by a discontinuous increase in pressure, density, temperature and entropy and by a discontinuous decrease of velocity and Mach.

Oblique Shock Wave

A oblique shock wave occurs when the streamlines cross the shock with an angle with respect to the incoming flow [5]. The flow across the oblique shock wave undergoes a weaker compression so that the flow keeps its supersonic state but with lower intensity with respect to the freestream. The fundamental relations for the oblique shock wave are:

$$\rho_2 V_{n2} = \rho_1 V_{n1} \tag{2.9}$$

$$p_2 + \rho_2 V_{n2}^2 = p_1 + \rho_1 V_{n1}^2 \tag{2.10}$$

$$(E_2 + p_2)V_{n2} = (E_1 + p_1)V_{n1} \tag{2.11}$$

$$V_{t2} = V_{t1} \tag{2.12}$$

The freestream Mach number is substituted by the normal freestream Mach number, therefore it is possible to obtain the Mach number downstream the shock wave in the following way:

$$M_2 = \frac{M_{n2}}{sin(\beta - \Theta)} \tag{2.13}$$

A final equation that links the shock angle β, the streamline deflection Θ and the shock intensity is necessary to close the problem.

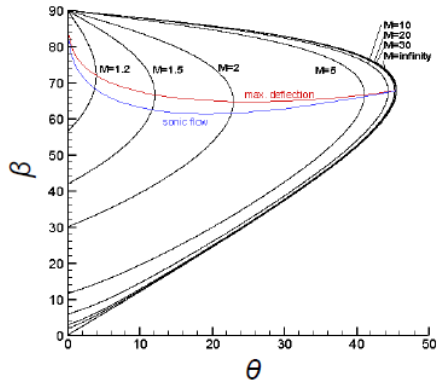

$$\frac{tan(\beta - \Theta)}{tan\beta} = \frac{2 + (\gamma - 1)M_1^2 sin^2\beta}{(\gamma + 1)M_1^2 sin^2\beta}$$

Figure 2.13: $\Theta - \beta - M$ Relation

2.3.2 Expansion and Compression Waves

Expansion Waves

The shock waves are not the only flow features in a hypersonic flow field. The shock is a strong compression that occurs when the flow deflects towards the freestream itself. An expansion occurs when the flow deflects away with respect to the direction of the freestream itself. Therefore, the other hypersonic phenomenon is the supersonic expansion given the wall deflection that rotates the flow such that is turned away with respect to the impinging flow. When the expansion generated leads to a continue deflection without energy dissipation through elementary expansion waves, the expansion is an isentropic evolution. Typically, the expansions form an expansion fan which is called Prandtl-Meyer expansion. The expansion waves diverge with respect to the compression waves, which generally intersect producing a shock wave. The width of the expansion fan is given by the relation between the angles of the first and the last elementary Mach wave and the wall deflection [5].

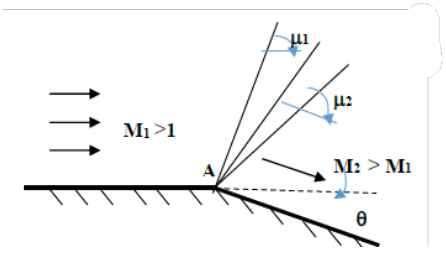

$$\nu(M) = \int \frac{\sqrt{M^2 - 1}}{1 + \frac{\gamma - 1}{2} M^2} \frac{dM}{M}$$

Figure 2.14: Prandtl-Meyer Integral

Compression Waves

The compression waves are generated due to the deflection of the wall, which turns toward the flow with respect to the freestream direction. In the supersonic regime, if the compression is generated by a corner, a shock wave will be produced. If the geometry change is smoother, such as when the wall is curved, a fan of converging compression waves of the same family will be generated, producing a shock as soon as two characteristics of the same family interact. It is possible to distinguish two types of compression waves. The left-turning compression waves occur when the wave is turned clockwise, and the right-turning when the wave is turned counterclockwise[5].

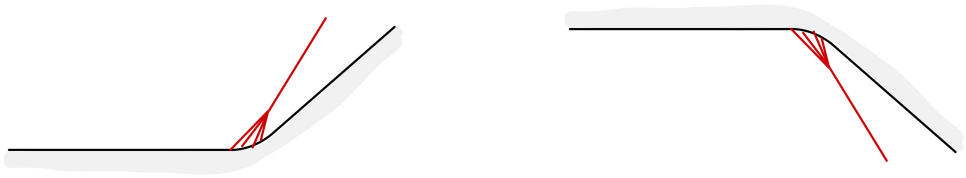

(a) Left Turning **(b)** Right Turning

Figure 2.15: Converging compression waves and related shock wave

2.3.3 Bow Shock

Bow Shock - $\Theta > \Theta_{max}$ Wall Deflection

Considering a flow impinging on a geometry with a first left turning and then a second right turning deflection. The nature of the shock changes according to the inclination angle of the wall with respect to the freestream direction. For $\Theta < \Theta_{max}$, where Θ_{max} is the maximum allowable inclination when the Mach tends to infinity, the shock is a classical oblique shock wave. The flow field downstream the shock is subsonic in a restrict region until the sonic line. As the increasing of the wall deflection, the shock becomes a curve shock wave and the region downstream the shock is no more uniform but it expands in subsonic. Also the expansion due to the right turning deflection is not uniform and the streamlines are curve and convergent [4]. The shock intensity decreases from the impact point moving downstream. When $\Theta > \Theta_{max}$, the shock is not able to deflect the flow and it becomes a curve-detached shock wave. Close to the corner the shock is normal and the region between the shock and the body is called shear layer. The shock shape and its distance from the body depend on the geometry and the freestream Mach. The distance from the body is defined as stand off distance and it decreases as the Mach increases [1].

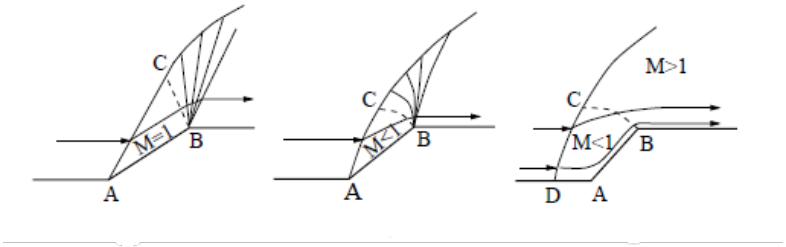

Figure 2.16: Bow Shock - Increasing Θ

Bilig Correlation

The flow is not isentropic and is composed by subsonic and supersonic regions, therefore the solution can be obtained only through numerical studies. For simple geometries with the hypothesis of perfect gas, the Bilig experimental correlation explains the dependency of the stand off distance with the geometry considered [4]. However, these are only simplifications because in hypersonic the temperature is high and can lead to phenomena as vibrational excitation and atomic ionization. For a sphere or cone:

$$\frac{\Delta}{R} = 0.143 e^{\frac{3.24}{M_{inf}^2}} \tag{2.14}$$

For a cylinder or wedge:

$$\frac{\Delta}{R} = 0.386 e^{\frac{4.67}{M_{inf}^2}} \tag{2.15}$$

Bow Shock - Blunt Body

The curve and detached shock wave occurs also for blunt body geometries. The curvature radius at the leading edge gives the typical features of a blunt body. Close to the nose the shock is normal and the flow downstream is subsonic and aligned with the freestream direction; moving along the shock, the intensity decreases.

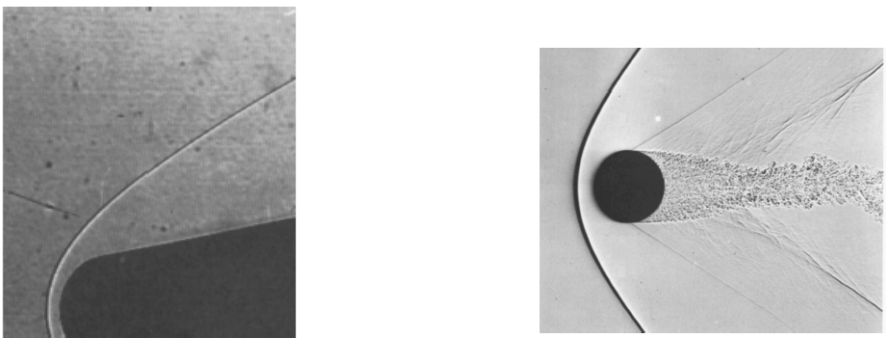

Figure 2.17: Images of bow shocks about blunt bodies

Stagnation Point

As explained, the hypersonic flow field are largely characterized by heavy heat fluxes, therefore the geometry of the body considered plays a crucial role to the management of the phenomena related to the high temperatures. Considering the Newtonian Theory, the pressure distribution over the surface of a body moving at very large Mach number is given by [1]:

$$Cp = 2cos^2\phi \tag{2.16}$$

With ϕ angle between freestream and the normal to the body; differentiating:

$$\frac{dp_e}{dx} = -2\rho_{inf}V_{inf}^2 cos\phi sin\phi \frac{d\phi}{dx} \tag{2.17}$$

From the Euler equation applied at the edge of the boundary layer:

$$\frac{dV_e}{dx} = -\frac{1}{\rho_e V_e}\frac{dp_e}{dx} \tag{2.18}$$

Therefore, close to stagnation point, where $cos\phi = 1$ and $sin\phi = \phi$ and rearranging:

$$q_w = \sqrt{\frac{dV_e}{dx}} \tag{2.19}$$

The stagnation point heat flux varies inversely with the square root of the nose radius; to reduce the heating, the nose radius must be large.

2.4 Newtonian Theory

The Newtonian theory describes the behaviour of a flow field in conditions of high Mach numbers. This theory is suitable for the description of the pressure distribution of bodies in hypersonic flow fields and allows to evaluate first approximations of forces and moments. The assumptions considered are: the fluid is composed by equal, non interacting and equidistant particles and the molecular agitation is neglected. The consequence is that when the flow interacts with the body, the component of the momentum normal to the wall goes to zero and a force normal to the wall is produced. The tangential component does not change and the flow follows the wall direction after the impact. Considering a flat plate at incidence, the pressure force on the wall depends only by the inclination of the surface with respect to local incidence of the particles. The drag of the body is determined only by the shape of the anterior part intercepted by the flow. The part behind is not considered by the theory and the difference with the freestream pressure is zero in this region [4].

2.4.1 Hypersonic Applications

For hypersonic flow, the theory provides acceptable results for Mach tending to infinite and Gamma to 1. In this case, a bow shock is generated and is closely attached to the body because at the increasing of the Mach the shock is deflected with lower inclinations and gets closer to the body. The disturbs caused by the body presence can not go back upstream at high Mach and the particles do not modify velocity and direction of the flow. This is explained precisely by the Newtonian theory, according to the force is only produced by the normal component of the momentum. In this case, the relations become:

$$\beta \to \Theta \tag{2.20}$$

$$Cp \to 2sin^2\Theta \tag{2.21}$$

The Newton hypothesis thus considers the particles as rigid spheres which exchange to the wall their momentum in the normal direction. Therefore, the fluid particles undergo a quick deviation given the inclination of the wall. This model is incorrect, in fact if the normal component of the momentum goes to zero, also the mass flux would. However, the mass flux is deflected in the tangential direction. As explained, for high Mach numbers the difference between the inclination angle and the wall inclination is minimum and the pressure coefficient is the same of the one predicted by the theory [4].

2.5 Hypersonic Governing Equations

In this section are proposed the normal and oblique shock waves relations and their variation for Mach tending to infinite.

2.5.1 Normal Shock Wave Relations

For a normal shock wave, the pressure, total pressure and entropy jumps tend to infinite; the density jump, the downstream Mach and pressure coefficient tend to an asymptotic value.

Density discontinuity relation

$$\frac{\rho_2}{\rho_1} = \frac{(\gamma+1)M_1^2}{2+(\gamma-1)M_1^2} \to \frac{\gamma+1}{\gamma-1} \tag{2.22}$$

Mach number

$$M_2^2 = \frac{2+(\gamma-1)M_1^2}{2\gamma M_1^2-(\gamma-1)} \to \frac{(\gamma+1)}{2\gamma} \tag{2.23}$$

Pressure coefficient

$$Cp = \frac{4(M_{inf}^2 - 1)}{(\gamma + 1)M_{inf}^2} \rightarrow \frac{4}{\gamma + 1} \tag{2.24}$$

Pressure discontinuity relation

$$\frac{p_2}{p_1} = \frac{2\gamma M_1^2 - (\gamma - 1)}{(\gamma + 1)} \rightarrow \infty \tag{2.25}$$

Temperature discontinuity relation

$$\frac{T_2}{T_1} = \frac{[2\gamma M_1^2 - (\gamma - 1)]\,[2 + (\gamma - 1)M_1^2]}{(\gamma + 1)^2 M_1^2} \rightarrow \infty \tag{2.26}$$

Entropy discontinuity relation

$$\frac{S_2 - S_1}{c_v} = ln\left[\frac{2\gamma M_1^2 - (\gamma - 1)}{(\gamma + 1)}\right] - \gamma ln\left[\frac{(\gamma + 1)M_1^2}{2 + (\gamma - 1)M_1^2}\right] \rightarrow \infty \tag{2.27}$$

Total Pressure discontinuity relation

$$\frac{p_2^o}{p_1^o} = \frac{p_2}{p_1}\left(\frac{1 + \frac{\gamma-1}{2}M_2^2}{1 + \frac{\gamma-1}{2}M_1^2}\right)^{\frac{\gamma}{\gamma-1}} \rightarrow 0 \tag{2.28}$$

2.5.2 Oblique Shock Wave Relations

Considering the case of an oblique shock wave with the Mach tending to infinite, the jump relations assume the following form. The pressure, temperature and entropy jumps tend to infinite; the density jump, the downstream Mach and pressure coefficient tend to an asymptotic value.

Pressure discontinuity relation

$$\frac{p_2}{p_1} = \frac{2\gamma M_1^2(M_1^2 sin^2\beta)}{(\gamma + 1)} \rightarrow \infty \tag{2.29}$$

Temperature discontinuity relation

$$\frac{T_2}{T_1} = \frac{2\gamma(\gamma - 1)}{(\gamma + 1)^2 M_1^2} sin^2\beta \rightarrow \infty \tag{2.30}$$

Density discontinuity relation

$$\frac{\rho_2}{\rho_1} = \frac{(\gamma + 1)M_1^2 sin^2\beta}{2 + (\gamma - 1)M_1^2 sin^2\beta} \rightarrow \frac{\gamma + 1}{\gamma - 1} \tag{2.31}$$

Pressure coefficient

$$Cp = \frac{4(M_{inf}^2 sin^2\beta - 1)}{(\gamma+1)M_{inf}^2} \rightarrow \frac{4}{\gamma+1} sin^2\beta \tag{2.32}$$

Where the Cp is not influenced by the Mach number for Mach tending to infinite.

Mach number

$$M_2^2 \rightarrow \frac{(\gamma+1)^2 - 4\gamma sin^2\beta}{2\gamma(\gamma-1)sin^2\beta} \tag{2.33}$$

$\Theta - \beta - M$ **Relation**

$$\Theta = \frac{2\beta}{\gamma+1} \rightarrow \beta = \frac{\gamma+1}{2}\Theta \tag{2.34}$$

Where the shock inclination is not influenced by the Mach number for Mach tending to infinite and is proportional to the wall deflection.

2.5.3 Oswatitsch Mach Number Independence Principle

At large Mach numbers, the force and moments coefficients lose the dependence with the Mach for a given geometry. As increasing the freestream Mach, for fixed freestream density and velocity, the solution in a finite fixed domain freezes into a limiting configuration where the shock shape is independent from the Mach [1]. Considering the normalized Euler equations, with respect to reference density, velocity, pressure, temperature, entropy and time, these do not change with the variation of the Mach. Moreover, after the normalization, the Euler equations and the boundary conditions formally maintain the original formulation.

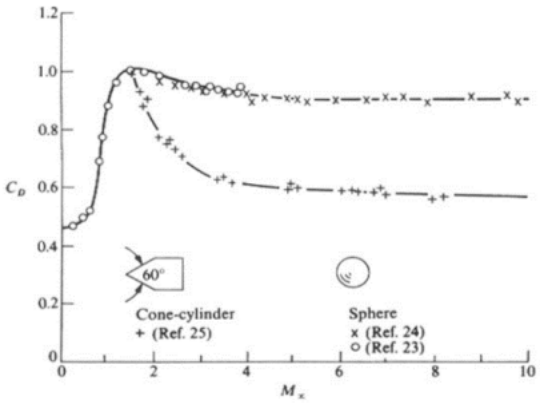

Figure 2.18: Oswatitsch Mach Number Independence Principle

For a blunt body in a hypersonic flow, the freestream conditions are given by the post shock conditions. If the freestream Mach tends to infinite:

Density discontinuity relation

$$\frac{\rho_2}{\rho_1} = \overline{\rho_2} = \frac{(\gamma+1)}{(\gamma-1)} \tag{2.35}$$

Tangential Velocity discontinuity relation

$$\frac{u_2}{V_{inf}} = \overline{u_2} = 1 - \frac{2sin^2\beta}{(\gamma+1)} \tag{2.36}$$

Normal Velocity discontinuity relation

$$\frac{v_2}{V_{inf}} = \overline{v_2} = \frac{sin2\beta}{(\gamma+1)} \tag{2.37}$$

Pressure discontinuity relation

$$\frac{p_2}{\rho_{inf}V_{inf}^2} = \overline{p_2} = \frac{2sin^2\beta}{(\gamma+1)} \tag{2.38}$$

Chapter 3

Flow Features Detection Techniques

3.1 Sensors for Hypersonic Flows

The identification of flow features in hypersonic flows, such as shock waves, is influenced by the proximity of other high-speed phenomena[3]. Therefore, detection requires greater accuracy in hypersonic or high supersonic flow fields. The detection method proposed in this work is inspired by the Canny Edge Detection method for image processing[2], combined with fluid dynamics relations to obtain an "educated" selection. All the thermo-chemical phenomena associated with high temperatures are neglected in this work, as they would not impact the detection methods as far as fluid dynamic features such as shock waves, contact surfaces, strong expansions, and wakes are concerned. As a result, the detection of species concentration gradients, which might be desirable in some high-speed flow applications, is not considered in this work and is left for future developments.
Given the complexity of the flow field, the production of accurate results is closely related to the definition of the mesh. The goal of this work is to drive mesh refinement by defining sensors able to detect the aforementioned flow structures. In this chapter, some of the sensors developed in recent years within the scientific community are presented. Each sensor is based on physical conditions depending on the desired accuracy, efficiency, and simplicity.

3.1.1 Ducros Sensor

The Ducros Sensor[6] uses velocity divergence and vorticity to distinguish shocks from turbulence[7]. It is sensitive to velocity divergence even when vorticity is negligible[8], occasionally leading to wrongly detected shocks.

It is defined as:

$$\phi = \frac{(\nabla \cdot \mathbf{v})^2}{(\nabla \cdot \mathbf{v})^2 + (|\nabla \times \mathbf{v}|)^2 + \delta} \tag{3.1}$$

where δ is a small positive number included to prevent the division by zero.

3.1.2 Kanamori and Suzuki Sensor

Kanamori and Suzuki proposed a shock detector based on the method of characteristics[9]. It requires high computational cost, and the applicability of this scheme is limited to inviscid flows[10]. Furthermore, Kanamori and Suzuki extended their method to unsteady flows with a shock-fixed coordinate moving with the shock[11].

3.1.3 Fujimoto, Kawasaki and Kitamura Sensor

The sensor proposed by Fujimoto, Kawasaki, and Kitamura[3] is based on the Canny Edge Detection [2], an image processing method, applied to CFD solutions for two-dimensional viscous/inviscid flows by replacing the brightness value of digital images with pressure. Through a Canny Edge Detection based on pressure values, the method allows the detection of shock candidates where the magnitude of the pressure gradient reaches a local maximum value. Then, the application of the Rankine-Hugoniot conditions allows for a final check to select the definitive shocks.

3.1.4 Pagendarm and Seitz Sensor

Pagendarm and Seitz[12] proposed a shock detection method based on the maxima of the density gradient. The first and second derivatives of density are calculated in the direction of velocity:

$$\frac{d\rho}{dn} = \nabla\rho \cdot \frac{\mathbf{v}}{|\mathbf{v}|} \tag{3.2}$$

$$\frac{d^2\rho}{dn^2} = \nabla\left(\nabla\rho \cdot \frac{\mathbf{v}}{|\mathbf{v}|}\right) \cdot \frac{\mathbf{v}}{|\mathbf{v}|} \tag{3.3}$$

The iso-surface of $\frac{d^2\rho}{dn^2} = 0$ corresponds to the maxima or minima of the density gradient. The condition $\frac{d\rho}{dn} > 0$ corresponds to a shock wave, while $\frac{d\rho}{dn} < 0$ corresponds to an expansion wave. A final threshold is necessary to remove incorrect results in smooth flow regions.

3.1.5 Sensors proposed in this work

After studying the available scientific literature on hypersonic flow feature sensors, the detection system proposed in the present work combines classical image processing methods with gradient methods to detect the targeted flow field features. The flow field functions involved and the physical conditions imposed are discussed in detail in Chapters 4 and 5, where the definition and use of the sensors are discussed.

3.2 Filters

Filtering the solution is frequently necessary due to numerical oscillations and spurious regions, which lead to false detection results. In this section, plausible procedures to smooth irregular flow regions or remove high-frequency fluctuations are presented.

3.2.1 Gauss Filter

The Gaussian filter has been broadly used in image processing and computer vision for many years[13]. It is the most effective filter for removing noise with a circular mask constructed using a Gaussian two-dimensional function, as:

$$g(x, y) = \frac{1}{2\pi\sigma^2} e^{-(x^2+y^2)/2\sigma^2} \tag{3.4}$$

where σ, the standard deviation, determines the extent of smoothing. Due to its implementation complexity in STAR-CCM+ and high computational cost, this filter has been considered only for possible future improvements.

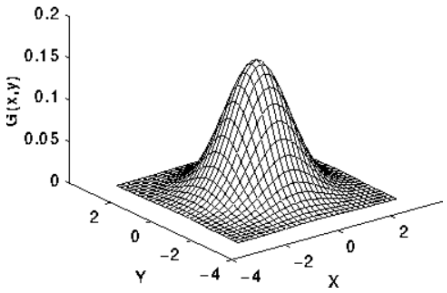

(a) Gauss Distribution

$$\frac{1}{273}\begin{bmatrix} 1 & 4 & 7 & 4 & 1 \\ 4 & 16 & 26 & 16 & 4 \\ 7 & 26 & 41 & 26 & 7 \\ 4 & 16 & 26 & 16 & 4 \\ 1 & 4 & 7 & 4 & 1 \end{bmatrix}$$

(b) Gauss Filter Mask

Figure 3.1: Gauss filter elements

Figure 3.1 shows a suitable integer-valued convolution kernel that approximates a Gaussian with a σ of 1.0. The approximation improves as the dimension of the kernel increases, but it becomes heavier in computational terms. For Gaussian smoothing, once the kernel has been defined, the convolution can be applied easily given the equation is separable in x- and y-components. The Gaussian is, in fact, the only completely circularly symmetric operator that can be decomposed in such a way.

3.2.2 Smoothing Filter

Smoothing filters are usually used to blur the image and reduce sharp variations. Mean filters apply an averaging process, replacing the value of each image pixel with the average of surrounding pixels. It is possible to directly apply this filter to CFD simulations by substituting the pixels with the domain's cells. If the signal is not uniform over one part of the neighborhood and rises in another part of it, the object will make itself the center of the neighborhood in the filtered image[14].

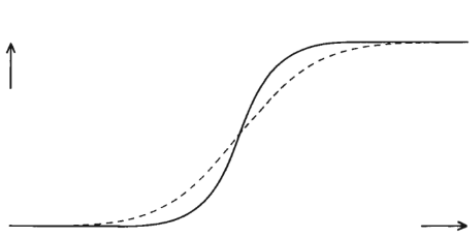

(a) Mean Filtering Operation

$\frac{1}{9}$	$\frac{1}{9}$	$\frac{1}{9}$
$\frac{1}{9}$	$\frac{1}{9}$	$\frac{1}{9}$
$\frac{1}{9}$	$\frac{1}{9}$	$\frac{1}{9}$

(b) Mean Filter Mask

Figure 3.2: Mean filter elements

The mean filter replaces each pixel value with the average value of its neighbors, including itself. In this way the unrepresentative pixel values are neglected. Often a 3×3 square kernel is used, as shown in Figure 1.4; larger kernels, i.e. 5×5 squares, can be used for more severe applications.

3.2.3 Thresholds

Thresholding operations are necessary to extract the desired flow features without interference from other phenomena. The objective is to define threshold values for normalized sensor variables for each case study.

3.2.4 Filters proposed in this work

The filtering operation proposed in this work is based on an absolute pressure condition, referring to the method designed by Wu Ziniu et al. in [11]. The flow field is modeled according to a thresholding condition related to the absolute pressure. The flow feature filtered is thus isolated and smoothed from the non-physical gradients provided by the detection. More details are provided in Chapters 4 and 5.

3.3 Adaptive Mesh Refinement Method

Adaptive Mesh Refinement (AMR) plays a central role in the application of the techniques described above in STAR-CCM+[15]. The capability to create the right mesh for CFD applications has a crucial impact on the resolution of the simulated flow fields. The AMR technique is generally adopted to refine the mesh in regions of interest for various applications, such as shock waves in aerodynamics, free surface interfaces between immiscible phases, and, in reacting flows, to resolve flame fronts[16]. The AMR technique is a dynamic method of mesh refinement that depends on the state of the solution[15]. Since it is an adaptive method, multiple simulations are necessary to progressively reduce the cell dimensions and reach the convergence of the solution. Each simulation starts with a new grid whose refinement is based on sensors arising from the previous solution, which is also interpolated into the new grid as an initial condition. The iterative process is repeated until the convergence criteria are met. The mesh generation process is a useful instrument to refine the flow field in the regions indicated by the refinement function, obtaining increasingly accurate solutions. The number of mesh generations depends on the problem and the specific mesh refinement function. There is an issue related to the computational cost and simulation time: a mesh refinement function that refines the flow field with too many cells can lead to slow simulations, while an excessively coarse refinement can affect the physics of the solution, leading to false and erroneous results.
The AMR method in STAR-CCM+ can be implemented in two different ways[17], namely Model-Driven Mesh adaptation, and User-Defined Mesh adaptation. The first option will not be considered in this work not only because the aim is to define the mesh manually but also because the Adaptive Mesh model works only for 3D cases in STAR-CCM+. The objective of the work is to drive the cell sizing by creating a user-defined function based on typical conditions that characterize discontinuities or fast variations in hypersonic flow fields. In this way, the grid can be refined in regions where selected flow field variables change rapidly, and coarsened in regions where the solution is smooth[18]. In particular, the refinement is driven by sensors able to detect specific hypersonic flow features.

The two steps are closely dependent; in fact, the user can set the mesh refinement according to the value of the sensor variables. This operation can be extended to all the sensors, leading to a global refinement function that refines the flow field only close to those fluid dynamics structures that the user wishes to detect.

3.3.1 Model-driven mesh adaptation

The dynamic mesh refinement method is an optional model directly implemented in STAR-CCM+, which can be selected from a list in the "Physics Continuum" folder under the name "Adaptive Mesh Refinement". The AMR method thus defined splits the cells at the center point: for rectangular trimmed cells, it splits the parent cell into 8 children cells, and for polyhedral cells, it splits them into 12-15 cells[16]. The AMR method implemented in STAR-CCM+ will not coarsen the original mesh, so it is suggested to start with an initial "coarse" mesh that still captures the flow characteristics.

(a) Rectangular Trimmed Cells **(b)** Polyhedral Cells

Figure 3.3: Types of cells in the AMR methods implemented in STAR-CCM+

This criterion is provided automatically from the STAR-CCM+ models [15]. The options available are the following.

Free Surface Mesh Refinement

This criterion is only valid when the Volume of Fluid (VOF) model is selected in the physics continuum and refines the free surface separating the two phases. This criterion is used in conjunction with the VOF multiphase model [15].

Overset Mesh Refinement

This criterion adapts the cell size of a lower priority region to the cell size of a higher priority region. In the case of one background region and one overset region, the cells of the background region are refined according to the overset region. This criterion is only valid after the creation of at least one overset interface [15].

Mesh adaptation for reacting flows

This criterion refines/coarsens cells in flame regions based on the second gradient of combustion scalar fields, such as species mass fractions, temperature, or progress variable. This criterion is only valid after a combustion model is selected [15].

3.3.2 User-Defined Mesh Adaptation

The user-defined mesh adaptation can be implemented defining, for example, a field function that returns an adaptation criterion based on the gradient of the Mach number. To capture discontinuities such as shocks, gradient of discontinuous solution scaled with the adaptation cell size is used [19]:

```
mag(grad(${MachNumber}))*(${AdaptionCellSize})
```

The quantity *AdaptionCellSize* returns the current cell size during the AMR procedure. Now it is possible to set in adaptation Request the number of refinement levels and the field function to refine the field. Maximum refinement level of 2 or 3 would be more realistic in order to reduce the computation time [19]. However, this AMR type combines the model-driven with the user-based adaptation and works for 3D volume mesh and not 2D meshes. Moreover, it requires a proper initial mesh able to capture the general flow characteristic since the method does not create the mesh but only split the cells and the surface mesh of the initial mesh must represent the geometry sufficiently well since no surface reconstruction is supported. Therefore, the work created for this work is based directly on a refinement field function without including the Adaptive Mesh option in the physics model. The refinement function is put in the XYZ Internal Table and is assigned to the Mesher in the Automated 2D Mesh option. In this way the simulations are executed depending on this function and the refinement occurs depending on the law chosen. The figures show the cell's differences between the initial weak sizing and the final refined sizing [17].

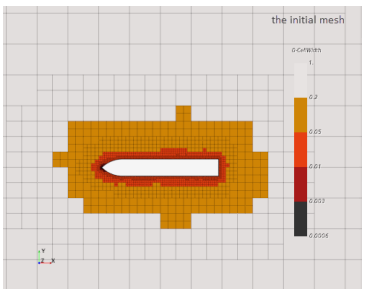

Figure 3.4: Coarse Initial Mesh

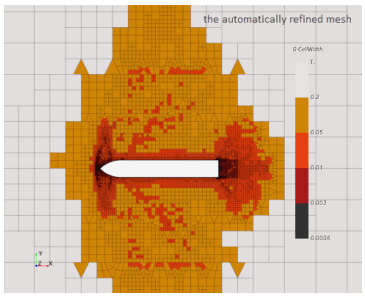

Figure 3.5: Final Refined Mesh

3.4 Canny-Edge Detection

The Canny-Edge detection is a common image processing method for detecting discontinuities in brightness. The process is divided into the following steps: smoothing, a first smoothing operation removes the noises and prepares the field for the successive phase; intensity gradients, phase related to the research of the brightness gradients to detect the image's edge; non-maximum suppression, the next step is the suppression of the lowest gradients to consider only the highest values; double threshold, the final check requires a double threshold to isolate only the definitive edges neglecting the false results.

3.4.1 Smoothing

The Gauss filtering operation is used as the first step of the process to remove the noises in the original image that can affect the detection.

3.4.2 Intensity Gradients

The second step is to find the image edges computing the brightness intensity gradients. The typical algorithms to define the gradients are the Sobel and Prewitt.

Sobel Operator

The Sobel operator performs a two-dimensional spatial gradient measure on images. This edge detector utilizes a pair of 3×3 convolution masks [20], one to estimate gradients in the horizontal direction and the other one to estimates gradients in the vertical direction. Sobel masks is defined as [21]:

-1	-2	-1
0	0	0
1	2	1

-1	0	-1
-2	0	2
-1	0	1

Table 3.1: Sobel Operator

Prewitt Operator

The Prewitt operator is like Sobel but with different coefficients of the mask [22]:

1	1	1
0	0	0
-1	-1	-1

-1	0	1
-1	0	1
-1	0	1

Table 3.2: Prewitt Operator

Considering the Sobel mask, the next step is to apply the kernel to the source image through an inner product calculation between the operator and the approximated gradients on the cell (i,j) [3].

$$dx_{ij} = \begin{bmatrix} -1 & 0 & 1 \\ -2 & 0 & 2 \\ -1 & 0 & 1 \end{bmatrix} \cdot \begin{bmatrix} a_{i-1,j+1} & a_{i,j+1} & a_{i+1,j+1} \\ a_{i-1,j} & a_{i,j} & a_{i+1,j} \\ a_{i-1,j-1} & a_{i,j-1} & a_{i+1,j-1} \end{bmatrix} \tag{3.5}$$

$$dy_{ij} = \begin{bmatrix} 1 & 2 & 1 \\ 0 & 0 & 0 \\ -1 & -2 & -1 \end{bmatrix} \cdot \begin{bmatrix} a_{i-1,j+1} & a_{i,j+1} & a_{i+1,j+1} \\ a_{i-1,j} & a_{i,j} & a_{i+1,j} \\ a_{i-1,j-1} & a_{i,j-1} & a_{i+1,j-1} \end{bmatrix} \tag{3.6}$$

Then, it is possible to compute the gradient magnitude and direction such that:

$$d_{ij} = \sqrt{dx_{ij}^2 + dy_{ij}^2} \tag{3.7}$$

$$\Theta_{ij} = tan^{-1}\left(\frac{dy_{ij}}{dx_{ij}}\right) \tag{3.8}$$

3.4.3 Non-Maximum Suppression

The non maximal gradient values are excluded in this phase. For each cell, it is checked if the gradient magnitude is maximal among pixels in the considered gradient direction. Then, the edge direction which is considered perpendicular to the gradient direction can be defined [3].

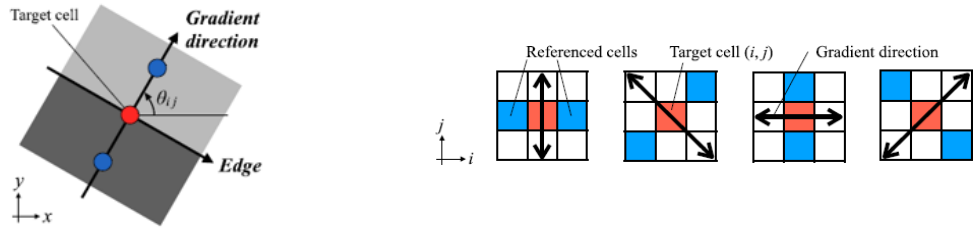

Figure 3.6: Edge Definition - Gradient Direction

The algorithm executed to distinguish edge pixels from the others compares the edge magnitude value of the target pixel with those of the pixels in the positive and negative gradient directions; if it is the largest compared to the pixels with the same direction in the mask, the target pixel is extracted as an edge candidate [3].

3.4.4 Double Threshold

In order to filter the undesired edges, a pair of thresholds, one is higher T_H and the other is lower T_L, determines [3]:

- $d_{ij} > T_H$: as an edge
- $d_{ij} < T_L$: as non edge
- $T_H < d_{ij} < T_H$: as an edge if more than one edge cells determined when $d_{ij} > T_H$ exist in the eight surrounding cells of the current cell

Figure 3.7: Original Image

Figure 3.8: Canny-Edge Detection

In the present work the output quantity of interest is not the brightness intensity. The flow variable used for the detection are the pressure or the Mach number. The process used for the detection refers to the Canny-Edge in terms of research of gradients. The aim is to find the highest value of the pressure or Mach gradients because they signs the transition across a hypersonic discontinuity. The sensor defined for the detection, in fact, are based on the specific nature of the flow features as shock and expansion waves. In this way, the suppression of the minimum values is executed isolating only the high gradients and the final thresholding operation define accurately the range of values where the fluid structure is detectable. The smoothing step is not necessary in the CFD applications and it can influence the physics of the problem; however in the complex cases the numerical fluctuations are relevant and can be removed with a filter application.

3.5 Case Studies

In this section are presented the case studies. The purpose of the simulations is to test the sensors and also verify the compatibility between the features expected from theory and the CFD results. The simulations are executed on inviscid and viscous cases. In this way a comparison between similar geometries highlights the different behaviour of the flow field.

Inviscid	**Viscous**
Ramp	Flat Plate
Blunt Body 1	Blunt Body 2
Shock - Shock Interaction	Shock - Boundary Layer Interaction
-	Wake

Table 3.3: Case Studies

Respectively, the first case has a simple geometry and the flow field is well known; the second simulates a bow shock around a ramp with the exceeding of the critical slope for the inviscid case and a blunt body for the viscous case; the third recreates the complex case of shock - shock interactions for the inviscid case and shock - boundary layer interaction for the viscous case. In the last viscous case, the target is the wake given the boundary layer separation from a cylindrical body. The final objective is to obtain a general formulation of the sensors derived by the results of the analysis conducted to drive the mesh refinement.

3.6 Inviscid Case Studies

3.6.1 Ramp

First simple inviscid test case. The flow field is well known in all the domain. An oblique shock wave is generated by the impact on the corner and a classical Prandtl-Meyer expansion fan is produced by the right turning corner. No entropy gradients affect the flow field and the region downstream the shock is uniform. The flow features are easily distinguishable, therefore the detection is well driven preliminarily with the Mach contours which highlight the oblique shock and the expansion fan with great accuracy. The simulation is started with a freestream Mach equal to 4, static pressure equal to 1000 Pa and temperature equal to 300 K. The expected flow features to detect are:

- Oblique Shock Wave: due to the impact on the corner
- Expansion Fan: due to the right turning wall

3.6.2 Blunt Body 1

Second inviscid test case. This case is more complex due to the exceeding of the critical slope that causes a bow shock and a large shear layer between the shock and the corner. The geometry is the same of the first case with the exception of the increase of the inclination angle of the wall which causes the detached shock. The irregularities of the flow field downstream the bow shock and the relevance of the entropy gradients in all the flow field affect the solution. Moreover, the region close to the sonic line is characterized by strong perturbations and numerical impurities. However, given the strong perturbations, the detection is not easily implementable especially as regards the expansion, which is different from the Prandtl-Meyer fan. The simulation is started with a freestream Mach equal to 4, static pressure equal to 1000 Pa and temperature equal to 300 K. The expected flow features to detect:

- Bow Shock: due to the exceed of the critical wall inclination
- Expansion: due to the right turning wall

3.6.3 Shocks Interaction

Third complex inviscid test case. The geometry is composed by two corner with different inclination, therefore this case is included in the shock - shock interactions. In fact, the double and different slope of the corners generates two oblique shocks which interact producing a third coalescent shock wave. Moreover, the intersection region generates a weak expansion wave reflecting to the wall and a slip line. The intersection point creates an irregular region, difficult to predict numerically. The detection of all the flow features is not standard and requires extreme precision. Moreover, the Mach number contours are not that accurate to recognize all the flow features and it is impossible to visualize the expansion and the slip line. The aim of the sensors creation, in fact, is to detect the fluid structures hidden in the interaction regions of complex cases. The simulation is started with a freestream Mach equal to 4.6, static pressure equal to 1000 Pa and temperature 300 K.
The expected flow features to detect are:

- Two Oblique Shock Waves: due to the different inclination of the corners
- Coalescent Shock Wave: due to the interaction between the two oblique shocks
- Expansion: generated by the triple point
- Slip Line: generated by the the triple point

3.7 Viscous Case Studies

3.7.1 Flat Plate

First viscous test case. As in the inviscid case, this case is simple due to the fact that the flow field is well known in all the domain. The flow interacts not only with the body but also with the displacement thickness generated the boundary layer. An oblique shock wave is generated by the impact on the boundary layer. Therefore, the presence of the boundary layer produces some spurious perturbations in the nose region, where the effects of the interaction between the boundary layer and the freestream are relevant. The boundary layer does not influence the shock detection. The simulation is started with a freestream Mach equal to 10, static pressure equal to 4.95 Pa and temperature equal to 52 K. The expected flow feature to detect is:

- Oblique Shock Wave: due to the impact on the boundary layer

3.7.2 Blunt Body 2

Second viscous test case. This test case simulates the flow around a cylindrical body that causes a curve and detached shock wave and a large shear layer between the shock and the nose. The irregularities of the flow field downstream the bow shock and the relevance of the entropy gradients in all the flow field affect the solution. Compared to the inviscid case, the expansion is not detectable with the same precision and accuracy. Therefore, the detection is not easily implementable and requires extreme attention. Moreover, the Mach number contours are not accurate to show the expansion as the curve shock wave. The presence of the boundary layer creates perturbations given the interaction with the other fluid structures. The simulation is started with a freestream Mach equal to 4, static pressure equal to 20.3143 Pa and temperature equal to 245.45 K.
The expected flow features to detect are:

- Bow Shock: due to the blunt body
- Expansion: due to the right turning cylindrical wall

3.7.3 Boundary Layer Shocks Interaction

Third complex viscous case. This test case presents a multiple shocks interaction which produces two coalescent shock waves, a weak expansion wave and a slip line, besides the oblique shock waves generated by the impact on the corner, the impact on the separation bubble and the subsequent reattachment of the flow. The effects of the boundary layer in this case are highly relevant. Moreover, the intersection region and the interaction between the expansion and the slip line make the detection process extremely complex. The expansion is weak and is not easily predictable. The simulation is started with a freestream Mach equal to 10, static pressure equal to 20.3143 Pa and temperature equal to 245.45 K.
The expected flow features to detect are:

- Oblique Shock Wave: due to the impact on the corner
- Oblique Shock Wave: due to the impact on the separation bubble
- Oblique Shock Wave: due to the flow reattachment to the wall
- Two Coalescent Shock Waves: due to the interaction between the separation and reattachment shocks (outer and inner)
- Weak Expansion Wave: generated by the triple point
- Slip Line: generated by the triple point

3.7.4 Wake

In the last viscous case is simulated a flow impinging on a cylindrical body in order to capture the wake behind the body. A large bow shock is formed on the nose and two reattachment shocks are developed behind the body to deflect the flow in the direction of the freestream. These oblique shock waves become evanescent moving downstream the domain where the expansions deflect the streamlines in parallel to the freestream. The simulation is started with a freestream Mach equal to 10, static pressure equal to 4.63422 Pa and temperature equal to 217.45 K.
The expected flow features to detect are:

- Bow Shock: due to the blunt body
- Oblique Shock Waves: due to the flow reattachment
- Expansion Waves: due to the turning walls
- Wake: due to the boundary layer detachment

Chapter 4

Model Creation

In this chapter is proposed the model creation. The model includes simultaneously two phases given their strong connection. The final model is well set if both the functions are defined properly:

- Adaptive Mesh Refinement
- Sensors

As introduced, the purpose is to create a mesh refinement function based on the sensors used for the detection. Therefore, the refinement is optimum if the sensors are well defined. Moreover, the typical hypersonic flow features, as the shock wave, are well detected if the mesh refinement level is proper.

4.1 Mesh

The meshing is crucial in the pre-processing phase for the resolution and accuracy of the solution. The meshing process in STAR-CCM+ starts with the initial creation of the grid with the volume mesh command which places raw elements. The second step includes the generation of a specific type of element:

- Triangle - 2D
- Quadrilateral - 2D
- Tetrahedron - 3D
- Hexahedron - 3D
- Arbitrary Polyhedron - 3D

The choice depends on the convergence velocity, the time of mesh creation and the memory available to store the data.

4.1.1 Mesh Types

Structured Mesh

The cells are quadrilateral in 2D or hexahedron in 3D and are insufficient for complex cases. The structured mesh can be ordered in regions or blocks where the mesh is structured. In this way it is possible to refine the domain only if required. In general the refinement occurs in the regions with strong gradients.

Unstructured Mesh

The cells do not follow any order and the geometry type is generally polygonal in 2D and polyhedral in 3D. The unstructured mesh are proper for complex cases.

Hybrid Mesh

This mesh type combines the cells according to the needs, typically triangles and quadrilaterals in 2D, prism and pyramids in 3D. A prism layer is used close to the wall, especially for Navier Stokes applications to simulate the boundary layer, with a growing thickness from the first layer to the last.

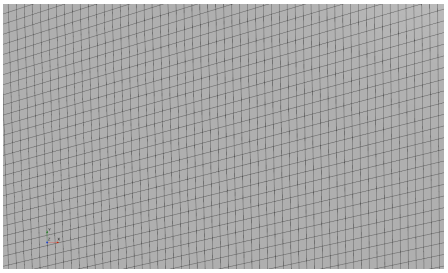

Figure 4.1: Structured Mesh

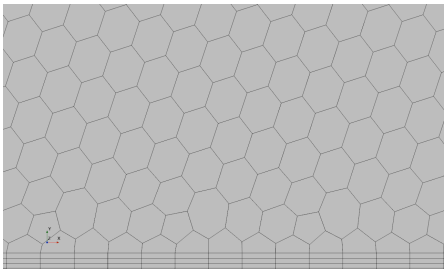

Figure 4.2: Unstructured Mesh

High-speed CFD calculations often rely on structured meshes to facilitate aligning the mesh with shocks. However, creating shock-aligned structured meshes with complex geometries and/or multiple interacting shocks is challenging [18]. The weak shock wave resolution and the misalignment of the mesh could introduce non-physical entropy gradients that contaminate the flow leading to numerical phenomena represented by Carbuncle [18] [23]. For the present work an unstructured mesh is set given its adaptability to complex geometries.

4.1.2 Mesh Quality

The measures of the mesh quality are the Skewness, which gives a measure of the cell's deviation from an ideal cell, the Smoothness, a measure of dimension variations between adjacent cells, the Aspect Ratio, ratio between the dimension of the longest edge and the dimension of the shortest edge. For the work it is preferred an Automated 2D Mesh which creates polygonal mesh in the domain and a prism layer close to the wall to simulate the boundary layer. In this way the mesh is generated by the software every time the user gives the input of mesh generation with the properties set in the controls. The meshers set are:

- Polygonal Mesher: it is directly related to the XYZ Internal Table where is assigned the Mesh Refinement function to size the grid according the established law
- Prism Layer Mesher: for the boundary layer, it is set with Geometric Progression as stretching function and Wall Thickness as Distribution Mode

4.1.3 Default Controls in STAR-CCM+

The software STAR-CCM+ allows to define manually the cells' property through controls related to the application of the automated mesh. The user can model these parameters in order to reach the better shape for the mesh according to the mentioned requirements.

Base Size

It refers to a characteristic dimension of the model and it is a reference value for the definition of the other parameters. This parameter can be used to scale the other mesh parameters. It is possible to regulate the mesh resolution changing the value of the base size: a lower value allows a better refinement with low dimension elements, while an higher value makes the grid coarse. In the work a value equal to 1 cm is set.

Target Surface Size

It refers to the edges length of the cells. It specifies the desired dimension of mesh elements generated on the model surface. This parameter is crucial for the mesh resolution. The target surface size allows to define a more detailed dimension for the surfaces, allowing a better precision in the simulation of complex geometries. In the work is Relative to Base as size type and a Percentage of Base equal to 100.

Minimum Surface Size

It refers to the minimum value of the edges length. This parameter set an inferior limit to the dimension of the elements and allows to prevent the creation of elements with extremely low dimensions. If the target surface size imposes a desired cells size, the minimum surface size set the limit to not overcome. In the work is Relative to Base as size type and a Percentage of Base equal to 10.

Surface Growth Rate

It refers to the velocity of cells growth towards the center of the volume at each step. It is important to manage the transition between elements of different dimensions. A grow rate equal to 1.2 means that each successive element will be 20% larger than the previous. Therefore, a proper surface grow rate ensures a gradual transition between elements and reduces the creation of warp cells. In the work a value equal to 1.3 is set.

Number of Prism Layers

It refers to the parameter that regulates the number of layer of prisms. The prism payers are used to capture the strong gradients close to the wall, especially for viscous applications, and are aligned perpendicularly to the surface. For the inviscid test case a number of prism layers equal to 2 is set; the number set for viscous cases depends on the problem.

Prism Layers Wall Thickness

It refers to the total height of the prism layers from the model surface towards the center of the volume. The growth of the layers can be controlled by the Prism Layer Stretching to manage the dimension variation between the layers. In the work a prism layer near wall thickness equal to 0.5 mm is set.

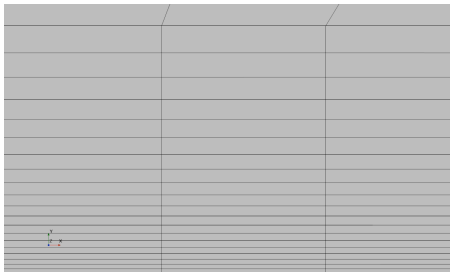

Figure 4.3: Prism Layers

4.2 Adaptive Mesh Refinement

The core of the work about the definition of the mesh refinement functions is now presented. The mesh could be based on a function defined by the user, thus the objective is to set up the run-mesh operations according to the mesh refinement function defined. In this way, after each simulation, the flow fields is refined to reach the convergence state. Changing the mesh refinement function and executing the simulation allows the user to monitor manually the meshing state. The mesh refinement functions defined during the work are the following.

Gradient Based Mesh Refinement

The first function is based on the gradient of flow features as pressure or the Mach number. The cell's dimensions is set depending on the gradient value.

Sensor Based Mesh Refinement

The second mesh refinement function is an upgrade of the former and is related directly to the sensors in order to refine the grid only close to the desired region.

Definitive Mesh Refinement

The definitive function is a combination of the previous ones. The final aim is to refine uniformly all the flow field, following the sensors based refinement for the targeted features and the gradient based refinement for the other regions.

4.2.1 Gradient Based Mesh Refinement

The preliminary mesh refinement function is based on the logarithmic magnitude of the pressure, or the Mach, gradient. The idea is to create a function that places the minimum size cells in regions where the logarithmic magnitude is higher than a threshold. In the other regions, the cell dimensions is established with the criteria defined by the function imposed. The function chosen is exponential type with geometric progression equal to 2. In this way the cells' size grow as approaching the regions with lower gradient values. This procedure, as briefly introduced in the first chapter, leaves extreme freedom to the user for a manually driven sizing.

The exponential function is so defined:

$$mesh_{ref,grad} = size_{min} \cdot 2^{\frac{log_{max}}{\Delta_{log}}} \cdot e^{-\frac{0.693}{\Delta_{log}} log_{10}(mag(grad(Pressure)))} \tag{4.1}$$

With:

- $size_{min}$: minimum cell size equal to 0.5 mm
- log_{max}: maximum value of $log_{10}(mag(grad(Pressure)))$
- Δ_{log}: step used to scale $log_{10}(mag(grad(Pressure)))$
- 2 and -0.693: parameters related to the geometric progression

Logarithmic Magnitude of Pressure Gradient

The $log_{10}(mag(grad(Pressure)))$ is defined as:

```
mag(grad(${Pressure})) > 0 ? log10(mag(grad(${Pressure}))) : -16
```

Logarithmic Magnitude of Mach Gradient

The $log_{10}(mag(grad(Mach)))$ is defined as:

```
mag(grad(${MachNumber})) > 0 ? log10(mag(grad(${MachNumber}))) : -16
```

An arbitrary value equal to -16 is set to avoid the cancellation when the logarithm goes to 0. The function is defined in a generalized form in the parameters $size_{min}$, Δ_{log}, log_{max}. However the parameter log_{max} strongly depends on the problem, limiting the application to each test case. This value is extrapolated arbitrarily by the user from the function $log_{10}(mag(grad(Pressure)))$. The case dependency related to the log_{max} parameter is removed through a normalization procedure of the logarithmic gradient functions. The procedure provides more simplicity to the sensors definition and is largely discussed in the sensor section.

4.2.2 Mesh Refinement Sensitivity Analysis

The mesh refinement depends on the cells placement established by the exponential function. In this terms, a sensitivity analysis has been conducted on a generic problem with the maximum value of $log_{10}(mag(grad(Pressure)))$ equal to 5. The Δ_{log} and $size_{min}$ are the changing variables and the cell's dimension is constantly doubled. As explained, each problem has its own maximum log value, while the variables are directly chosen by the user.
Examples of the mesh refinement functions created are:

- Mesh Refinement Δ_{log} 0.5 - $size_{min}$ 0.5 mm
- Mesh Refinement Δ_{log} 1 - $size_{min}$ 0.5 mm
- Mesh Refinement Δ_{log} 2 - $size_{min}$ 1 mm

Further analysis has been conducted following these criteria with geometric progression equal to 3 and using the logarithmic magnitude of the Mach gradient. The obtained results are quite similar except the application range due to the variation of the maximum log value.

Mesh Refinement Δ_{log} 0.5 - $size_{min}$ 0.5 mm

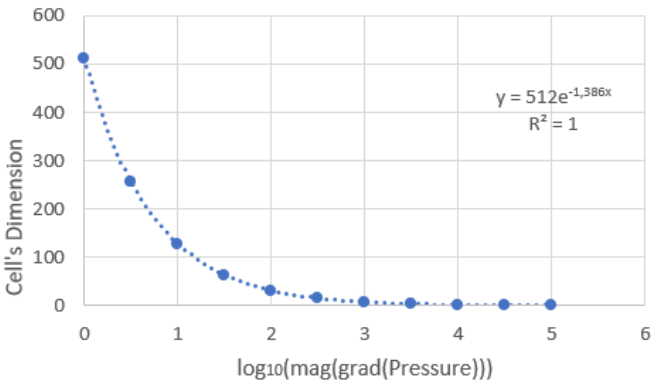

Cell [mm]	Log [/]
0.5	5
1	4.5
2	4
4	3.5
8	3
16	2.5
32	2
64	1.5
128	1
256	0.5
512	0

Figure 4.4: Mesh Refinement Δ_{log} 0.5 - $size_{min}$ 0.5

Mesh Refinement Δ_{log} 1 - $size_{min}$ 0.5 mm

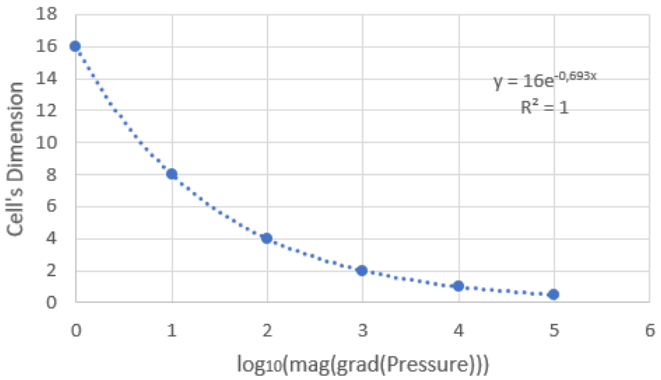

Cell [mm]	Log [/]
0.5	5
1	4
2	3
4	2
8	1
16	0

Figure 4.5: Mesh Refinement Δ_{log} 1 - $size_{min}$ 0.5

Mesh Refinement Δ_{log} 2 - $size_{min}$ 1 mm

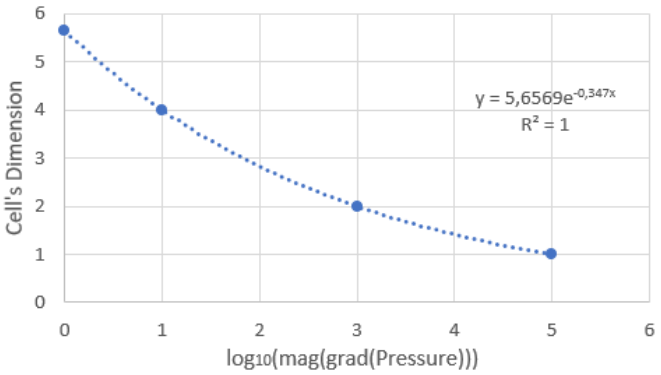

Cell [mm]	Log [/]
1	5
2	3
4	1
5.6569	0

Figure 4.6: Mesh Refinement Δ_{log} 2 - $size_{min}$ 1

Considering a trade off related to the computational cost and the refinement level, the mesh refinement function Δ_{log} 1 - $size_{min}$ 0.5 mm is selected. Too high grid dimension could generate incorrect results, while too small cells' size could lead to high computational costs. The choice is given by a combination of the requirements.

4.2.3 Sensor Based Mesh Refinement

As briefly discussed, the next step is to remove the case dependency for the definition of the mesh refinement function. The intention is to normalize the threshold imposed to the logarithmic pressure gradient removing the necessity to impose the maximum value for each problem. Therefore, the definitive mesh refinement function is now based directly on the sensor function, whose definition is largely proposed in the next section together with the normalization procedure. In this way is possible to refine the mesh according to the flow features targeted: for example, for the shock wave sensor is imposed a cell's dimension equal to the minimum size and at the same time a cell's dimension equal to an arbitrary value larger than the minimum in all the other regions. The function thus created refines the grid only around the shock wave. As in the first function defined, the values imposed for the refinement operation are set accordingly to the trade off of refinement quality and computational cost. Examples of the sensor based mesh refinement are here presented.

Shock Wave Mesh Refinement

```
${shock_sensor} == 1 ? ${csize_min} : ${csize_min}*4
```

- Shock sensor cell's size: minimum
- Other regions cell's size: 4 times minimum

Shock and Expansion Waves Mesh Refinement

```
${shock_sensor} == 1 ? ${csize_min} : ${csize_min}*4 && ${expansion_sensor} == 2 ? ${csize_min}*2  : ${csize_min}*16
```

- Shock sensor cell's size: minimum
- Other regions cell's size: 4 times minimum
- Expansion sensor cell's size: 2 times minimum
- Other regions cell's size: 16 times minimum

The trade off between the refinement level and the computational cost has a considerable impact in the velocity of the simulation. A too low cell's dimension could lead to high calculation time. Therefore, a different mesh refinement type is imposed between shock and expansion sensor in order to place more cells close to the shock where the gradients are stronger.

4.2.4 Definitive Mesh Refinement

Finally, the definitive mesh refinement is a combination of the previous ones. The function thus defined places a specific cell's dimension in the targeted regions and refines the other flow regions according to the exponential law based on the gradients variation. Examples of the definitive mesh refinement are here proposed.

Shock Wave Mesh Refinement

```
${shock_sensor} == 1 ? ${csize_min} : ${mesh_refinement_gradient}
```

- Shock sensor cell's size: minimum
- Other regions cell's size: exponential function based

Shock and Expansion Waves Mesh Refinement

```
${shock_sensor} == 1 ? ${csize_min} : ${mesh_refinement_gradient} && ${expansion_sensor} == 2 ? ${csize_min}*4 : ${mesh_refinement_gradient}
```

- Shock sensor cell's size: minimum
- Expansion sensor cell's size: 4 times minimum
- Other regions cell's size: exponential function based

In this way, the minimum cell's size is set for the shock wave and a specific dimension for the expansion; in all the other regions the sizing follows the exponential function based on the gradients. Therefore, the flow field refinement is uniform and now the mesh is properly refined for the detection phase of each flow structure. The user can choose the dimension to assign to the sensors regions according to the trade off between the refinement level, the computational costs and the case considered. This procedure could be extended to all the other sensors, creating a complete refinement function which includes all the flow features desired. The refinement is thus completely driven by the user. Finally, the combination of the two refinement function speeds up the convergence process. In fact, using the gradient based refinement, the flow features are refined according to the gradient intensity. Therefore the convergence state could be reached very slowly and more run-mesh are necessary to refine all the region targeted. The sensor based refinement is more efficient because the sensor detects the desired flow feature and the refinement thus defined works on all the cells indicated by the sensor. In this way the flow feature is refined with high accuracy only with few run-mesh operations.

4.3 Sensors

In this chapter is presented the sensors creation procedure. As introduced in the first chapter, the AMR method and the sensors definition are closely related because the detection works efficiently if the mesh is refined properly. The sensors creation refers to the Canny-Edge detection considering the gradient method combined with the specific physics of the flow features considered. The purpose of the work is to find a general definition suitable for each case treated.

4.3.1 Sensors Normalization

Before describing the sensors, a mention to the normalization process of the flow field functions is necessary. In details, the function used to the detection is often based on the gradient of quantity as pressure or the Mach number and this leads to the issue of finding the right gradient threshold, which depends on the case treated. The normalization executed removes this problem obtaining a more general formulation of the sensor function.

Normalized Pressure Gradient

```
(${log10(mag(grad(Pressure)))}-${Minimum Pressure})/(${Maximum Pressure}-${Minimum Pressure})
```

Normalized Mach Gradient

```
(${log10(mag(grad(Mach)))}-${Minimum Mach})/(${Maximum Mach}-${Minimum Mach})
```

In other words, a general function of $log_{10}(mag(grad(Pressure)))$ is defined scaling on a range from the minimum to the maximum value. In this way it is possible to remove the issue to find the exact value depending on the case. The sensors are created balancing the rate of the normalized gradients from 0 % to 100 %. Therefore, the objective is to define a general formulation considering only a range of the normalized gradients where the related flow feature is certainly detectable. The final range derived from the simulations for each sensor are proposed in the last section as a guide to the user approaching to a generic detection problem. The same procedure is applied to the Mach number depending on the feature to detect.

4.3.2 Shock Sensor

The shock sensor is created through the superposition of two effects. The first is related to the transition of the high-speed flows from supersonic to subsonic or low supersonic through a condition on the Mach normal to the shock. The second is related to the strong variation across the shock in terms of pressure or Mach gradient. The sensitivity analysis proposed in the next chapter shows which is the more proper variable to use for the shock or expansion detection.

Mach Normal Condition

A general oblique shock wave could be treated as a normal shock wave superimposed on a uniform flow [11]. The normal direction of shock wave is perpendicular to local Mach gradient or pressure, which is based on normal Mach number method proposed by Lovely and Haimes [24]; thus the normal Mach number can be obtained as the scalar product between the Mach vector and the Mach gradient:

$$M_n = \overline{M} \cdot \overline{\nabla M} \tag{4.2}$$

```
dot($${Velocity}/${SoundSpeed},$${grad(Mach)_norm})
```

The Mach vector is defined as the ratio between the velocity vector and the speed of sound; the Mach gradient is normalized with respect to its magnitude:

$$\overline{M} = \frac{\overline{V}}{sos} \tag{4.3}$$

```
$${Velocity}/${SoundSpeed}
```

$$\overline{\nabla M} = \frac{\nabla M}{|\nabla M|} \tag{4.4}$$

```
mag(grad(${MachNumber})) > 0 ? grad(${MachNumber})/mag(grad(${MachNumber})) : [1,0,0]
```

Therefore, the Mach gradient, which is a vector, indicates the direction of the gradient variation and the scalar product with the Mach vector returns in output the local Mach normal. The objective is to find the Mach parallel to the gradients given the orthogonality to the shock wave and verify the variation from supersonic to subsonic or low supersonic. The Mach normal range is negative because the pressure increases through the shock and the Mach gradient is opposite.

Gradient Condition

After the definition of the Mach normal and the normalized logarithmic magnitude of pressure gradient, the shock wave function is created as a combination of the two functions. In fact, the Mach normal is necessary to rate the transition from supersonic to subsonic and the logarithmic pressure gradient is modelled to consider only the highest gradients. The sensor thus defined is created according to a thresholding operation on the two conditions. The threshold ϵ depends on the problem, however, the normalization process allows to define a general value of each problem because the quantities are scaled in all their application range.

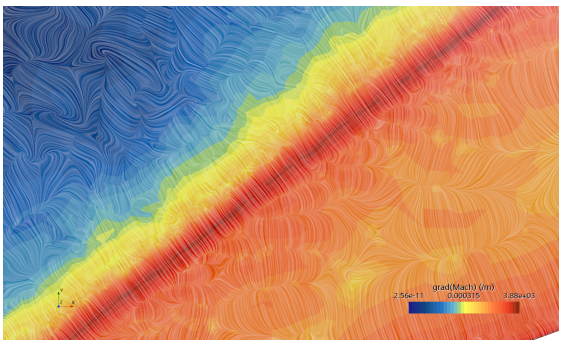

Figure 4.7: Mach Gradient - Shock Wave

Sensor Proposed

The general formulation is given by a superposition of the two conditions:

$$shock_{sensor} = (-\epsilon_1 < \overline{M_n} < -\epsilon_2) + (\nabla p_{norm} > \epsilon) \tag{4.5}$$

As explained, the Mach normal condition extract a range of negative values due to the pressure increase and Mach decrease through the shock wave. The threshold on the normalized pressure gradient is high in order to capture only the highest flow discontinuities which occur exactly across the shock. The optimum range are proposed at the end of the results chapter.

4.3.3 Expansion Sensor

The expansion sensor is defined with the same procedure of the shock sensor with the difference detailed in the following subsection.

Mach Normal Condition

The range of the Mach normal is now positive given the fact that the flow increases its velocity through the expansion. The flow undergoes a supersonic expansion where the pressure decreases and the Mach increases. Therefore, it rates a velocity increase across the expansion.

Gradient Condition

As regards the gradient condition, the gradients are less intense, thus the expansion is well detected with a lower percentage. As shown in the sensitivity analysis, for the expansion sensor the logarithmic gradient of the Mach captures the related flow feature with a better resolution. However, despite the spurious oscillations provided to the flow field, the pressure gradient is more sensible to the flow variations. In fact, the detection of this particular structure is not universally defined and in the complex cases the pressure gradient is preferred to the Mach.

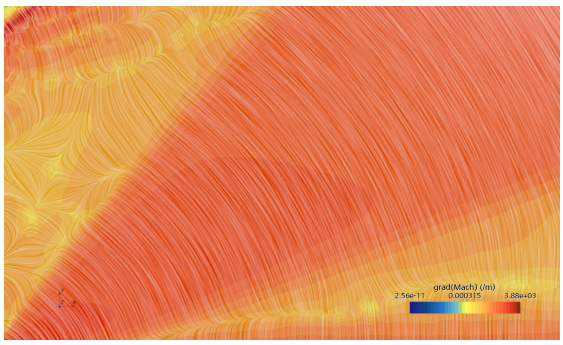

Figure 4.8: Mach Gradient - Expansion Wave

Sensor Proposed

The general formulation is given by a superposition of the two conditions:

$$expansion_{sensor} = (\epsilon_1 < \overline{M_n} < \epsilon_2) + (\nabla M_{norm} > \epsilon) \tag{4.6}$$

As explained, the Mach normal condition extract a range of positive values due to the pressure decrease and Mach increase through the expansion wave. The threshold on the normalized gradient is lower than the shock wave because the gradients are less intense for the expansion.

4.3.4 Slip Line Sensor

The slip line detection is the more complex due to the interaction with the shock and expansion waves. The slip line separates region with different Mach, temperature, density but same pressure and same velocity direction. This phenomenon occurs because the flow moves across different shock and develops the features mentioned to respect the tangency and the freestream conditions. Therefore, the Mach normal condition is not used for this sensor, which is composed by two gradient conditions.

Gradient Conditions

The objective is to find that region where the pressure gradient is minimum or lower than a certain threshold and the Mach gradient is quite relevant. The sensor is thus created with a combination of the two conditions.

Sensor Proposed

The general formulation is given by a superposition of the conditions:

$$slip_{sensor} = (\nabla M_{norm} > \epsilon) + (\nabla p_{norm} < \epsilon) \tag{4.7}$$

The threhsold imposed for the two normalized gradients is not the same and requires a precise analysis to be obtained. In the complex case a smoothing operation can be necessary to remove the numerical impurities.

4.4 Wake Sensor

The wake, or the region where the boundary layer detaches from the body, is a large region where the total temperature changes strongly with respect to the shock waves where it does not change compared to the freestream. The wake is accurately detected with the only condition based on the normalized total temperature. The normalization is executed directly on the total temperature, scaled with respect to its maximum and minimum, and not with the logarithmic magnitude of the quantity. A sensor based on the logarithm of the total temperature is more sensible and severe in the detection, and it leads to the capture of undesired features in the shocks region and strong numerical oscillations close to the nose. The threshold imposed is set in order to exclude the highest values related to the freestream.

Sensor Proposed

The general formulation is thus defined:

$$wake_{sensor} = T^{o}_{norm} < \epsilon \tag{4.8}$$

4.5 Filter

The detection process leads to numerical oscillations and false Mach distribution in the flow field. Given the regular nature of the expansion, a filtering operation is applied to remove the spurious gradients far from the expansion region. In fact, if the shock wave is that thin layer of sharp variations, the expansion is a more uniform region where the gradients change smoothly. However in the complex case the spurious gradients derived also from the other sensors are removed with the smoothing process. The filtering method is based on the filter proposed by Wu Ziniu and others [11]:

$$|\nabla p| = \epsilon \frac{p_{abs}}{l_n} \tag{4.9}$$

With ϵ filtering threshold, p_{abs} absolute pressure and l_n local mesh size. This filter takes account of the local mesh size and pressure, thus it can yield better result in complex flow [11]. The filter proposed for the work executes a cut on the flow field through a thresholding operation on the normalized absolute pressure. The threshold imposed is strongly problem dependent and changes without prediction depending on the case.

Filter Proposed

The general formulation is thus defined:

$$filter = p_{abs,norm} < \epsilon \tag{4.10}$$

Where the absolute pressure is normalized with respect to its maximum and minimum value. The filtering operation is secondary with respect to the detection because the numerical errors are never too relevant. In the result chapter are proposed the solutions with the filter applied to the detection only to have a better visualization. In fact, the expansion sensor works with a great efficiency and the results are acceptable also without the filtering condition.

Chapter 5

Simulations Settings

In this chapter are proposed the simulations settings necessary to the subsequent definition of the sensors functions. For each case are presented the condition used to capture the flow features and the related application range. The final results are shown in the next chapter where are proposed the scenes of the sensors and the definitive mesh refinement functions.

5.1 Sensitivity Analysis - Shock and Expansion

A sensitivity analysis is conducted on a simple test case with the purpose to select the optimum parameters for the sensors definition. In particular, this procedure is executed for the definition of the shock and expansion sensor. The slip line sensor requires a different approach due the complexity of the flow structure.

Sensitivity Analysis - Gradient

The first analysis concerns the use of the gradient for the detection of shock and the expansion wave. The choice is between the normalized gradient of Mach number or pressure.

Sensitivity Analysis - Mach Number

The second is conducted changing the Mach number in order to evaluate the optimum range of the gradient percentage. The analysis are conducted using the Mach and pressure gradient for each Mach considered.

Possible future analysis could be conducted substituting the other condition imposed on the Mach normal with the pressure normal to the shock. As explained, the normal direction of shock wave is perpendicular to local pressure gradient [24], thus the normal pressure can be obtained following the same procedure.
The simulations are set with the following parameters:

- Shock Sensor - Mach Normal: range between -1.5 and -0.5
- Expansion Sensor - Mach Normal: range between 0.5 and 2
- Shock Sensor - Gradients: 10 % highest values
- Expansion Sensor - Gradients: 25 % highest values

5.1.1 Pressure Gradient

Shock Sensor

```
${Mach_norm}> -1.5 && ${Mach_norm}< -0.5 && ${log10(mag(grad(Pressure)))_norm} > 0.9 ? 1: 0
```

Expansion Sensor

```
${Mach_norm}> 0.5 && ${Mach_norm}< 2 && ${log10(mag(grad(Pressure)))_norm} > 0.75  ? 2: 0
```

5.1.2 Mach Gradient

Shock Sensor

```
${Mach_norm}> -1.5 && ${Mach_norm}< -0.5 && ${log10(mag(grad(Mach)))_norm} > 0.9 ? 1: 0
```

Expansion Sensor

```
${Mach_norm}> 0.5 && ${Mach_norm}< 2 && ${log10(mag(grad(Mach)))_norm} > 0.75  ? 2: 0
```

The following scenes do not include the filtering operation in order to show the differences in terms of resolution.

5.1.3 Mach 3

Pressure Gradient

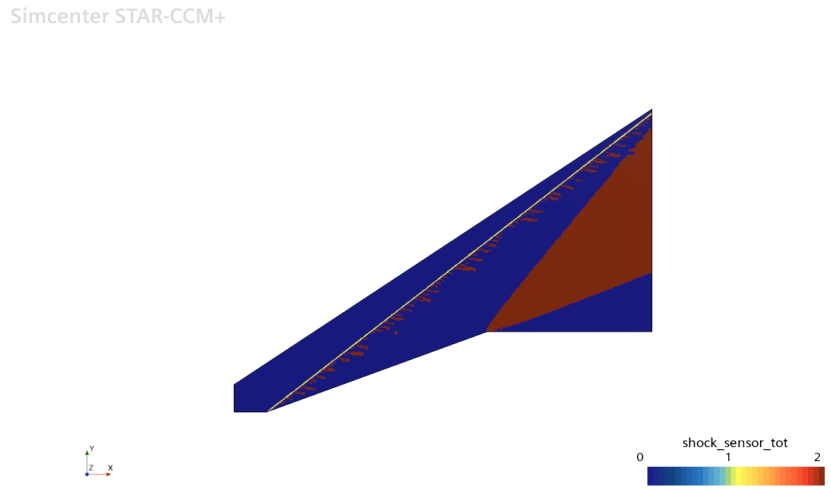

Figure 5.1: Pressure Gradient - Mach 3 Sensors - Ramp

Mach Gradient

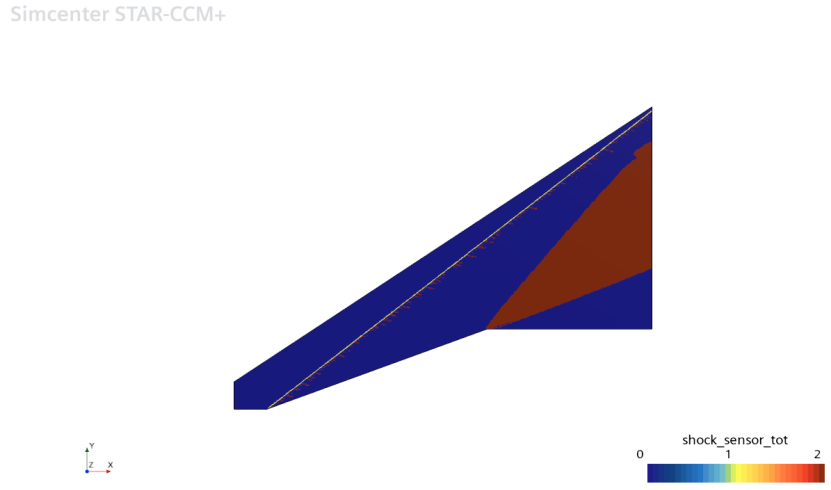

Figure 5.2: Mach Gradient - Mach 3 Sensors - Ramp

5.1.4 Mach 5

Pressure Gradient

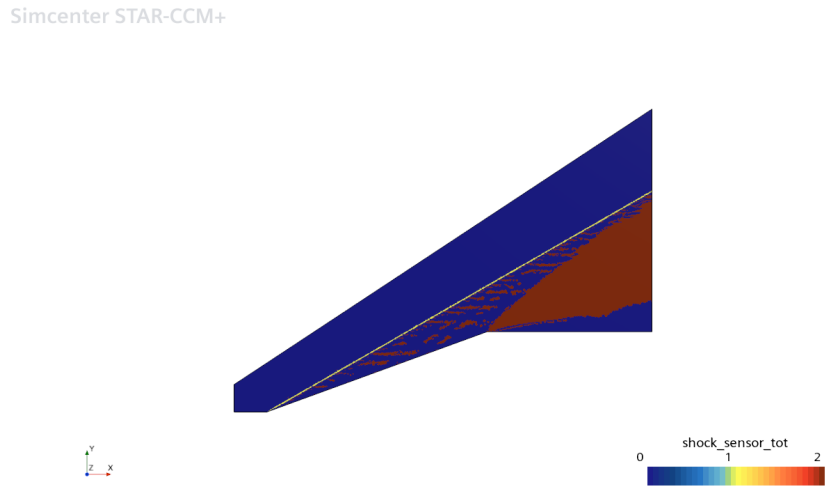

Figure 5.3: Pressure Gradient - Mach 5 Sensors - Ramp

Mach Gradient

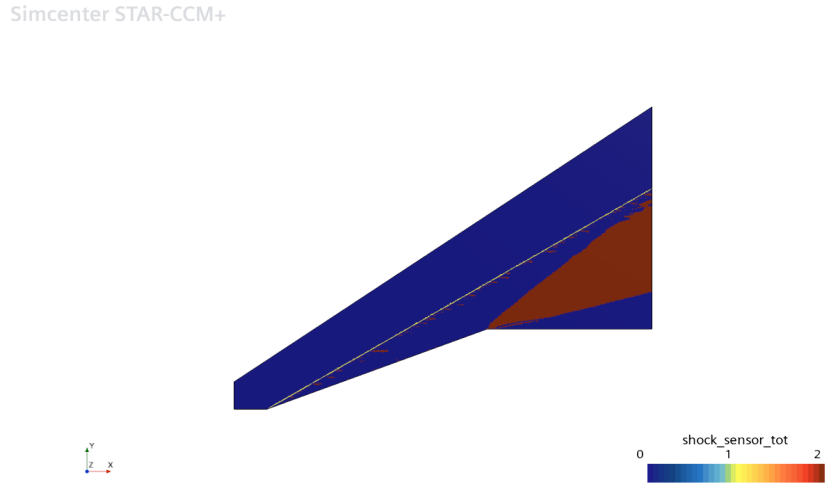

Figure 5.4: Mach Gradient - Mach 5 Sensors - Ramp

5.1.5 Mach 7

Pressure Gradient

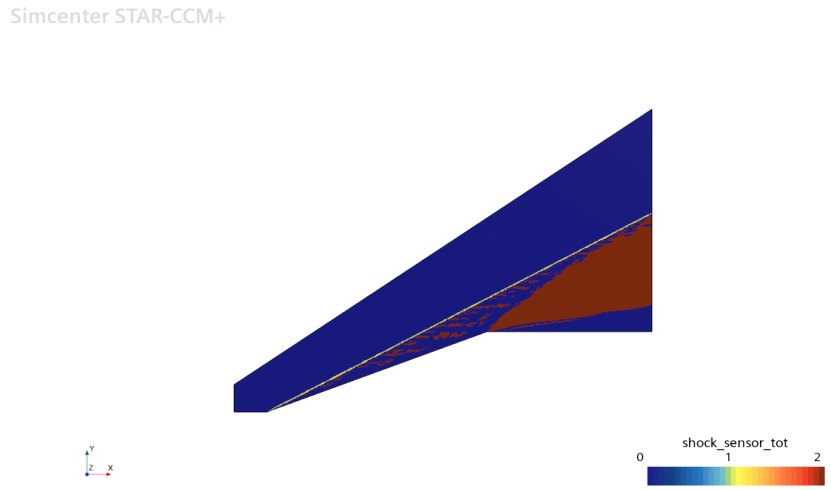

Figure 5.5: Pressure Gradient - Mach 7 Sensors - Ramp

Mach Gradient

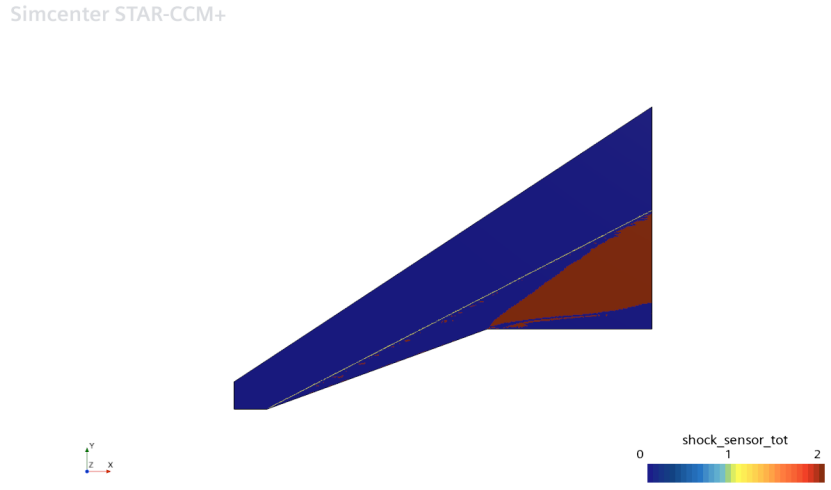

Figure 5.6: Mach Gradient - Mach 7 Sensors - Ramp

5.1.6 Mach 10

Pressure Gradient

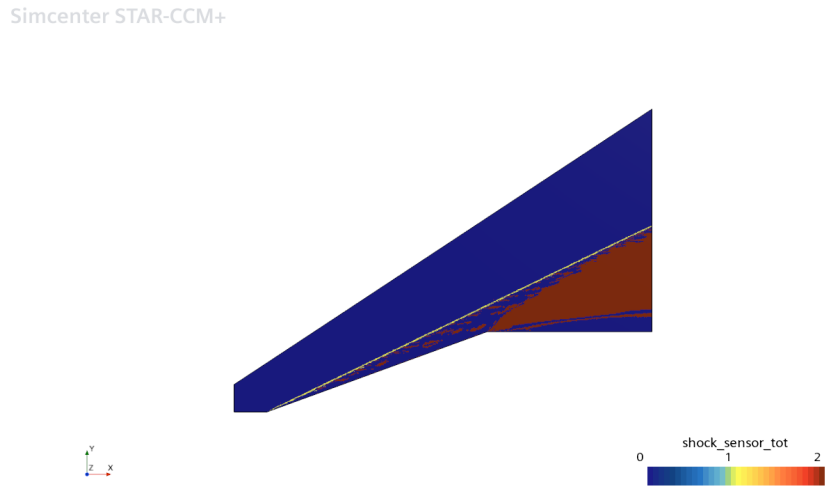

Figure 5.7: Pressure Gradient - Mach 10 Sensors - Ramp

Mach Gradient

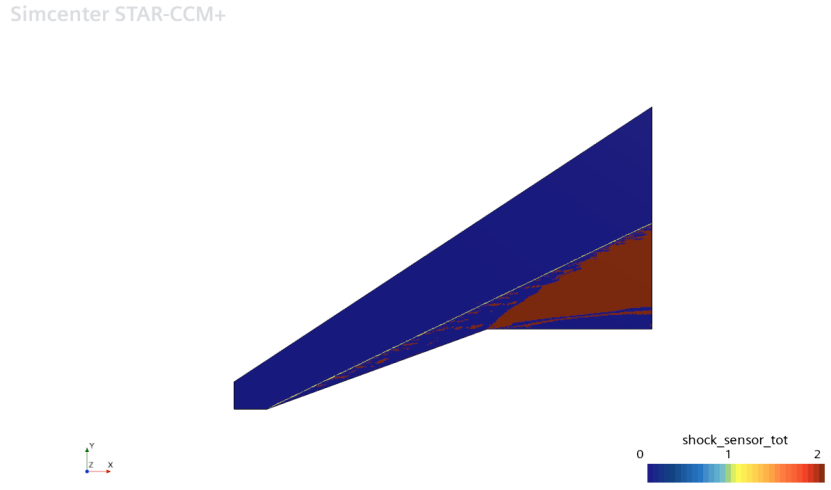

Figure 5.8: Mach Gradient - Mach 10 Sensors - Ramp

5.1.7 Sensitivity Analysis Results - Shock and Expansion

The analysis leads to the following results:

- The shock has a better resolution with the pressure gradient
- The expansion has a better resolution with the Mach gradient
- The preliminary parameters are acceptable

In detail, the detection range of the highest 10 % and 25 %, respectively for the shock and the expansion sensor, is optimum. The shock is captured within the 10 % highest gradients; the expansion, as expected, has a lower intensity and is well isolated with gradient values larger than 75 %. The Mach normal condition works efficiently with the starting range considered. In particular, for the shock sensor the negative range excludes all the other flow features and detects the shock region. For the expansion, the condition captures the increase in terms of velocity through the expansion. The combination of the conditions removes the numerical oscillations and shows the flow feature targeted. Moreover, this preliminary phase demonstrates that the conditions thus applied remove the problem related to the case dependent threshold. In fact, even changing the Mach with the same settings, the results obtained are more than acceptable. Furthermore, changing the rate of the of the gradients depending on the problem leads to better results. As regards the expansion sensor, for example, imposing a percentage from 75 % to 77.5 %, allows a better visualization of the related flow feature. As proposed in the final summary, the expansion presents a band of values where the detection works smoothly, despite the shock sensor which is always well detected around the 90 %. In the results sections are proposed the precise values used for each test case treated. In conclusion, for the shock sensor is imposed the condition on the pressure gradient and for the expansion sensor on the Mach gradient. However, as mentioned in the previous chapter, a specific discussion depending on the case is proposed for the expansion. The complex cases requires the pressure gradient, which is more sensible to the discontinuities when these are difficult to be detected.

5.2 Sensitivity Analysis - Slip Line

The slip line detection is not standard as for the shock and expansion waves. This flow feature has a different detection method which is based only on the normalized pressure and Mach number gradients. Therefore, sensitivity analysis are conducted changing the range of these variables. Moreover, the pressure changes significantly in all the flow field and using the pressure gradient normalized with respect to the freestream value could provide strong vibrations in the flow field. The normalized Mach does not affect the solution as the normalized pressure. The sensitivity analysis conducted consider two different approaches: the first includes all the range of the normalized gradients between their maximum and minimum values; the second consider a reduced range. In the last case, it is possible to consider a reduced range of both the maximum and minimum, or a reduced range with a reduction only of the minimum value.

Normalization - Maximum and Minimum

In this case, the range are not changed and the slip line and the other flow features are well detected with the following parameters:

```
${log10(mag(grad(Pressure)))_norm} < 0.875 && ${log10(mag(grad(Mach)))_norm} > 0.945 ? 2 : 0
```

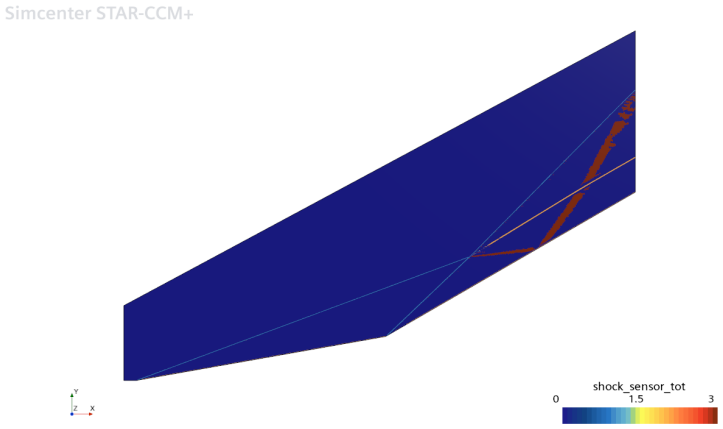

Figure 5.9: Normalization - Unchanged Range

Normalization - Maximum and Different Minimum

In this case, the maximum is not changed but the minimum of the normalized pressure gradient is set to a value equal to -2 from -12 and the minimum of the normalized Mach gradient is set to -3. The parameters imposed for the detection:

```
${log10(mag(grad(Pressure)))_norm} < 0.875 && ${log10(mag(grad(Mach)))_norm} > 0.945 ? 2 : 0
```

Normalization - Different Maximum and Different Minimum

In this case both the maximum and minimum value are reduced. The normalized pressure gradient is set to have the minimum from -12 to -2 and the maximum from 7 to 5.

```
${log10(mag(grad(Pressure)))_norm} && ${log10(mag(grad(Mach)))_norm} > 0.945 ? 2 : 0
```

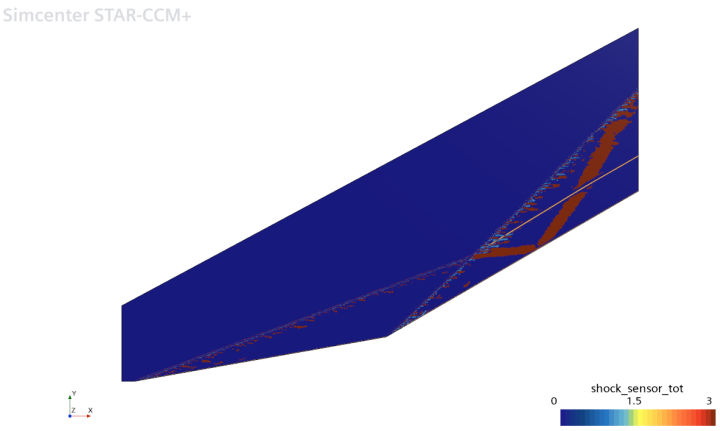

Figure 5.10: Normalization - Reduced Range

As clearly shown in the plot of the flow features sensors, the reduced range approach provides errors in the detection of the shocks because considering a lower maximum is equivalent to remove physical details about the highest gradients. Therefore, the reduced range approaches are strongly problem dependent and are mentioned as an useful way to the user for the detection of the slip line in case of complex cases. Thus the general method considering the normalization between all the pressure range is adopted. The approach where the maximum is unchanged and the minimum is modified can be applied because the difference is only in the parameters adopted for the slip line sensor definition.

5.3 Ramp

5.3.1 Shock Sensor

The shock is detected with the following parameters:

- Mach normal: $(-1.5; -0.5)$
- Normalized Pressure Gradient: $(> 90\%)$

Mach Normal Condition

The Mach normal condition is necessary to capture the transition from supersonic to subsonic flow through the shock. The range from -1.5 to -0.5 detects with high accuracy the shock. The spurious values are removed with the gradient condition.

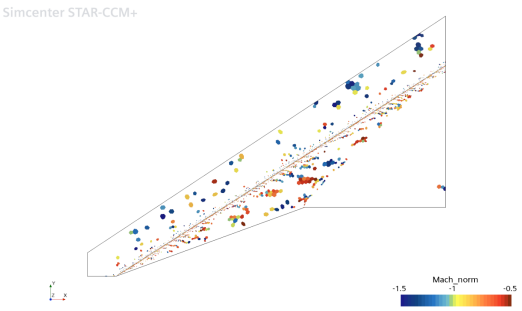

Figure 5.11: Mach Normal - Shock - Ramp

Gradient Condition

The shock is well captured within the 10 % of the highest values of the normalized pressure gradient. A cut above the 90 % isolates exactly the shock.

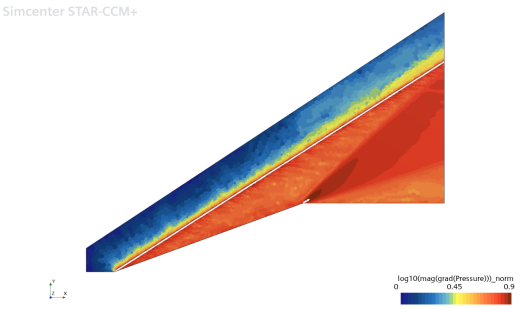

Figure 5.12: Pressure Gradient - Shock - Ramp

5.3.2 Expansion Sensor

The expansion is detected with the following parameters:

- Mach normal: (0.5; 2)
- Normalized Pressure Gradient: ($> 75\%$)

Mach Normal Condition

The Mach normal condition captures the velocity increase through the expansion.

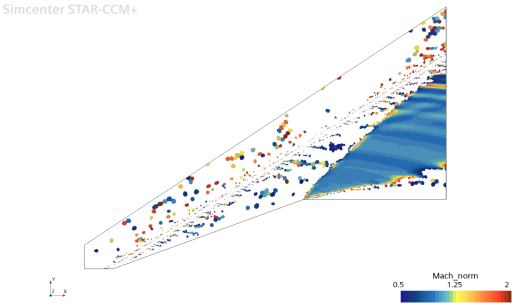

Figure 5.13: Mach Normal - Expansion - Ramp

Gradient Condition

The expansion is well detected within the 25 % highest gradients. The combination with the Mach normal condition isolates the expansion from the spurious gradients close to the shock region.

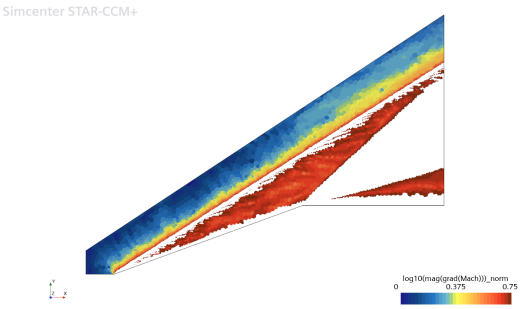

Figure 5.14: Mach Gradient - Expansion - Ramp

5.4 Blunt Body 1

5.4.1 Shock Sensor

The shock is detected with the following parameters:

- Mach normal: $(-3.5; -0.5)$
- Normalized Pressure Gradient: $(> 92.5\%)$

Mach Normal Condition

The Mach normal condition is applied with a larger range in order to achieve a better resolution in the detection.

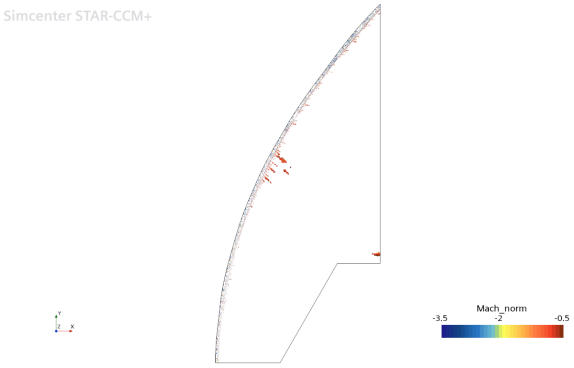

Figure 5.15: Mach Normal - Shock - Blunt Body 1

Gradient condition

The shock is well captured within about the 10 % of the highest values of the normalized pressure gradient. The rate equal to 92.5 % is a more accurate value.

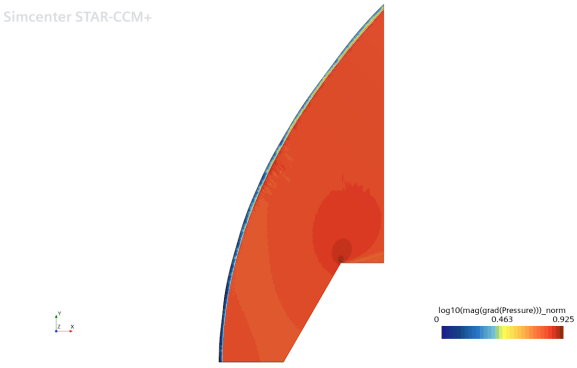

Figure 5.16: Pressure Gradient - Shock - Blunt Body 1

5.4.2 Expansion Sensor

The expansion is detected with the following parameters:

- Mach normal: (0.5; 2)
- Normalized Pressure Gradient: ($> 77.5\%$)

Mach Normal Condition

The Mach normal condition captures the expansion region and some sharp variations downstream the shock wave when the flow becomes supersonic again. Therefore, noises and numerical oscillations accumulates in the region close to the sonic line.

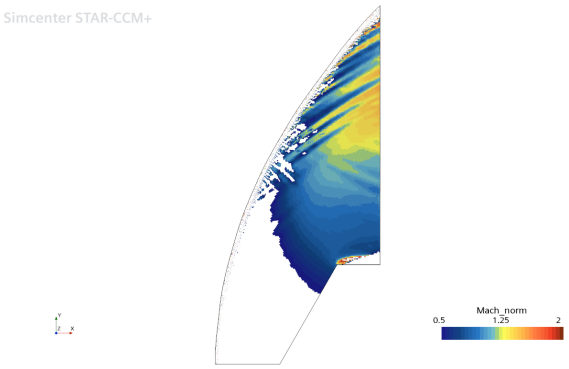

Figure 5.17: Mach Normal - Expansion - Blunt Body 1

Gradient Condition

The expansion and the impurities are well detected within the 22.5 % highest gradients.

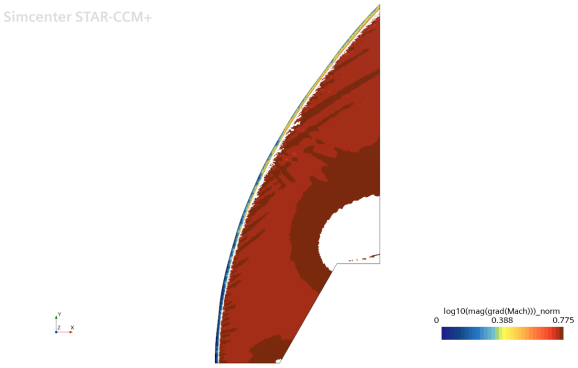

Figure 5.18: Mach Gradient - Expansion - Blunt Body 1

5.5 Shocks Interaction

5.5.1 Shock Sensor

The shocks are detected with the following parameters:

- Mach normal: $(-1.5; -0.5)$
- Normalized Pressure Gradient: $(> 92.5\%)$

Mach Normal Condition

The shocks are efficiently detected with the typical Mach normal range.

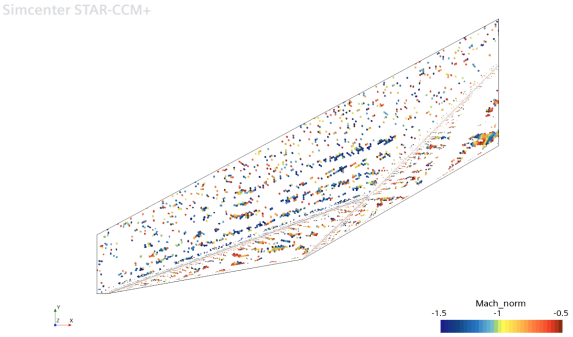

Figure 5.19: Mach Normal - Shock - Shocks Interaction

Gradient Condition

The shocks are well captured within the 10 % of the highest values of the normalized pressure gradient. The 92.5 % rate detects better the two oblique shock waves and the coalescent shock.

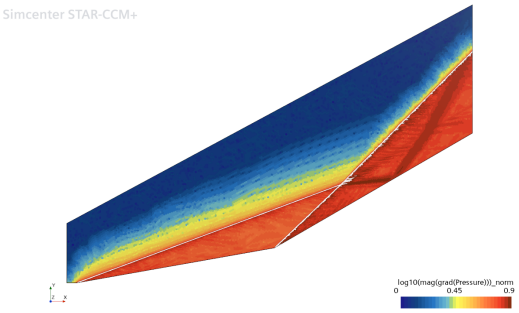

Figure 5.20: Pressure Gradient - Shock - Shocks Interaction

5.5.2 Expansion Sensor

The expansion is detected with the following parameters:

- Mach normal: (0.5; 2)
- Normalized Pressure Gradient: ($> 87.5\%$)

Mach Normal Condition

The expansion is efficiently detected with the typical Mach normal range.

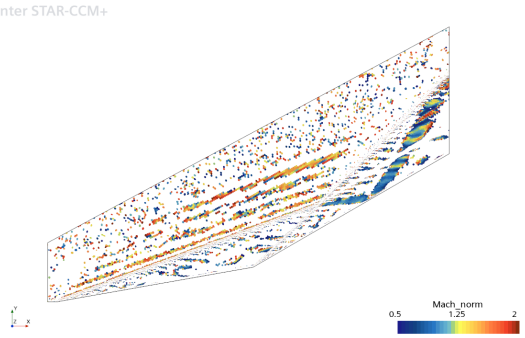

Figure 5.21: Mach Normal - Expansion - Shocks Interaction

Gradient Condition

The gradient intensity in this case is higher and equal to 87.5 %.

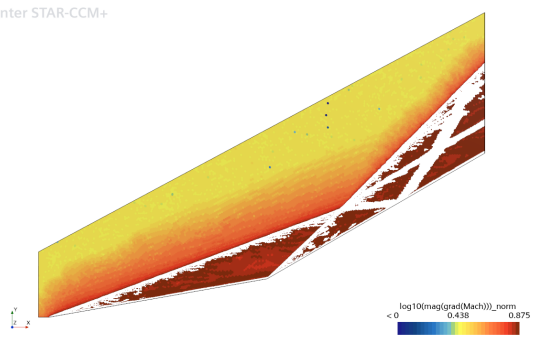

Figure 5.22: Mach Gradient - Expansion - Shocks Interaction

5.5.3 Slip Line Sensor

The slip line is detected with the following parameters:

- Normalized Pressure Gradient: ($< 87.5\%$)
- Normalized Mach Gradient: ($> 94.5\%$)

Pressure Gradient Condition

The minimum pressure gradient condition is highlighted with a cut below 87.5 %, where the slip line is captured. The gradients higher than the 87.5 % include the shocks and the expansion reflected to the wall.

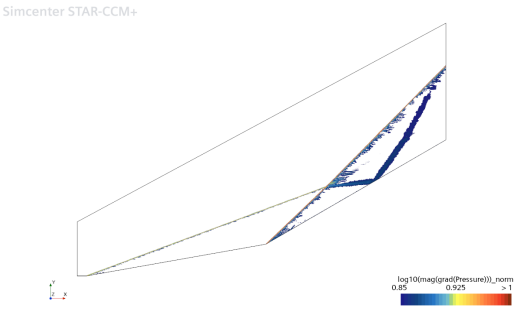

Figure 5.23: Pressure Gradient - Slip Line - Shocks Interaction

Mach Gradient Condition

A cut above the 95 % in the normalized Mach gradient excludes exactly the three shocks and the slip lines. In this way the slip line is detected within the 5 % of the highest Mach gradient values. Therefore, the combination with the pressure gradient condition captures exactly the slip line, excluding the other flow features.

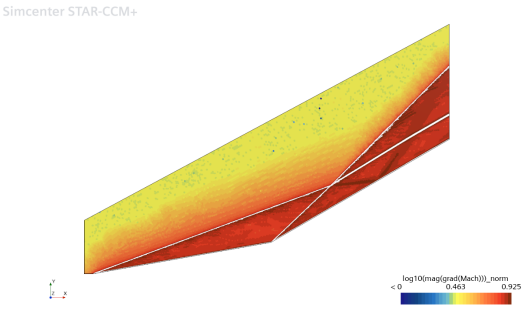

Figure 5.24: Mach Gradient - Slip Line - Shocks Interaction

5.6 Flat Plate

5.6.1 Shock Sensor

The shock is detected with the following parameters:

- Mach normal: $(-1.5; -0.5)$
- Normalized Pressure Gradient: $(> 90\%)$

Mach Normal Condition

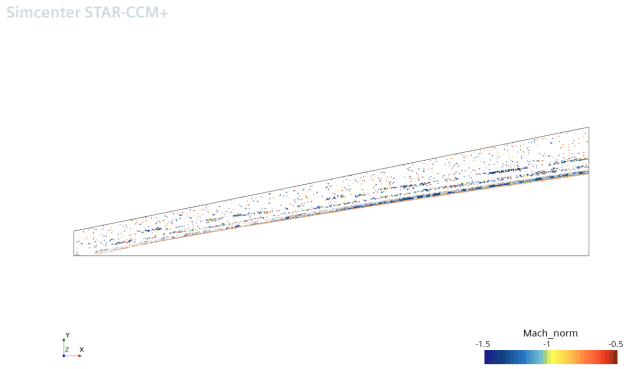

Figure 5.25: Mach Normal - Shock - Flat Plate

Gradient Condition

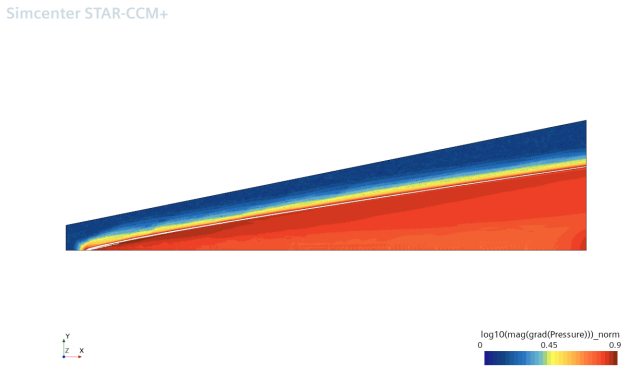

Figure 5.26: Pressure Gradient - Shock - Flat Plate

5.7 Blunt Body 2

5.7.1 Shock Sensor

The shock is detected with the following parameters:

- Mach normal: $(-3.5; -0.5)$
- Normalized Pressure Gradient: $(> 90\%)$

Mach Normal Condition

The Mach normal range is the same of the inviscid case.

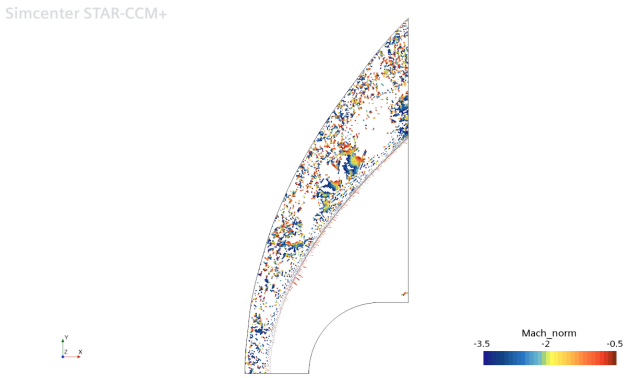

Figure 5.27: Mach Normal - Shock - Blunt Body 2

Gradient Condition

The bow shock is precisely captured within the 10 % highest gradients.

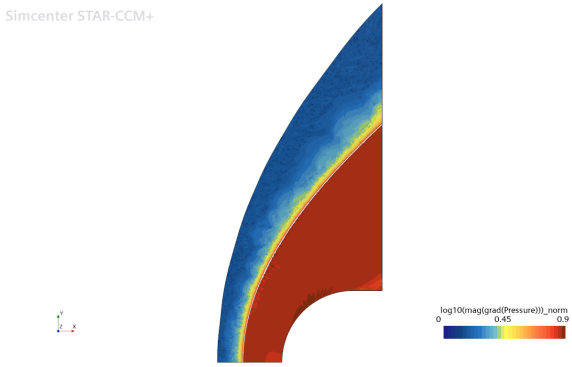

Figure 5.28: Pressure Gradient - Shock - Blunt Body 2

5.7.2 Expansion Sensor

The expansion is detected with the following parameters:

- Mach normal: (0.5; 2)
- Normalized Pressure Gradient: ($> 86\%$)

Mach Normal Condition

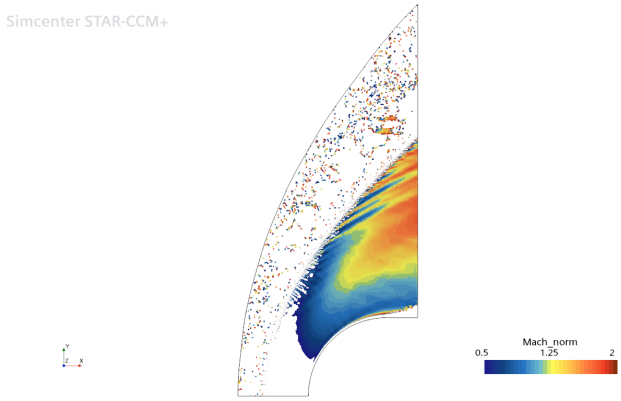

Figure 5.29: Mach Normal - Expansion - Blunt Body 2

Gradient Condition

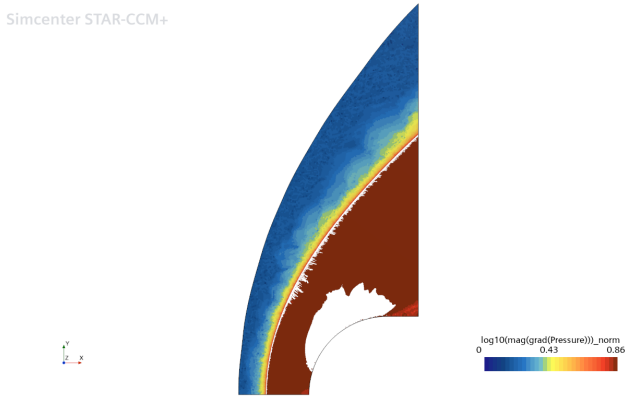

Figure 5.30: Pressure Gradient - Expansion - Blunt Body 2

5.8 Boundary Layer Shocks Interaction

5.8.1 Shock Sensor

The shocks are detected with the following parameters:

- Mach normal: $(-1.5; -0.5)$
- Normalized Pressure Gradient: $(> 86.5\%)$

Mach Normal Condition

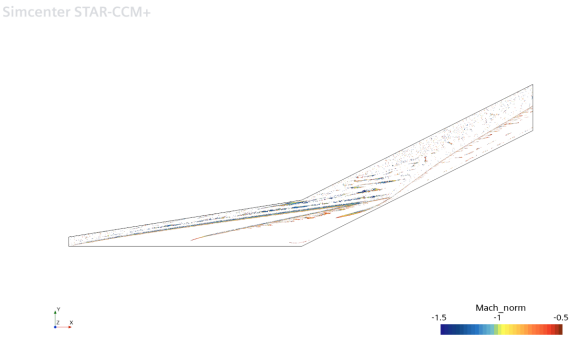

Figure 5.31: Mach Normal - Shock - Boundary Layer Shocks Interaction

Gradient Condition

The percentage applied for this case is lower than the standard used for the shock detection. In this way the shocks with lower intensity are well detected together with the strong shocks.

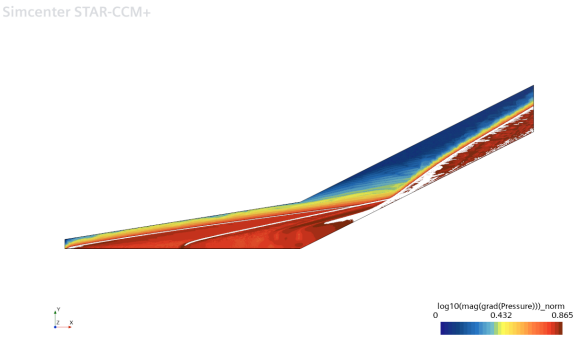

Figure 5.32: Pressure Gradient - Shock - Boundary Layer Shocks Interaction

5.8.2 Expansion Sensor

The expansion is detected with the following parameters:

- Mach normal: (0.5; 2)
- Normalized Pressure Gradient: ($> 85\%$)

Mach Normal Condition

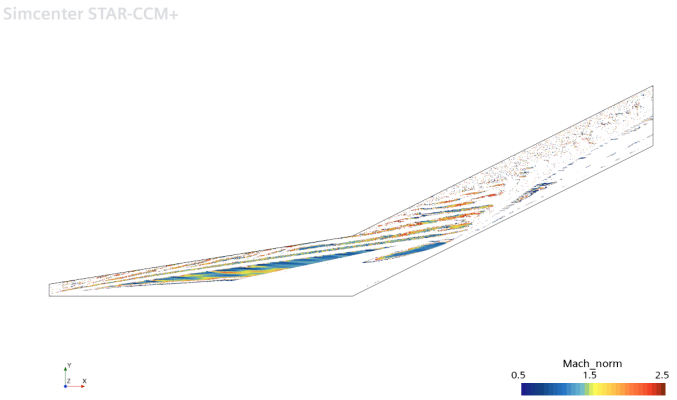

Figure 5.33: Mach Normal - Expansion - Boundary Layer Shocks Interaction

Gradient Condition

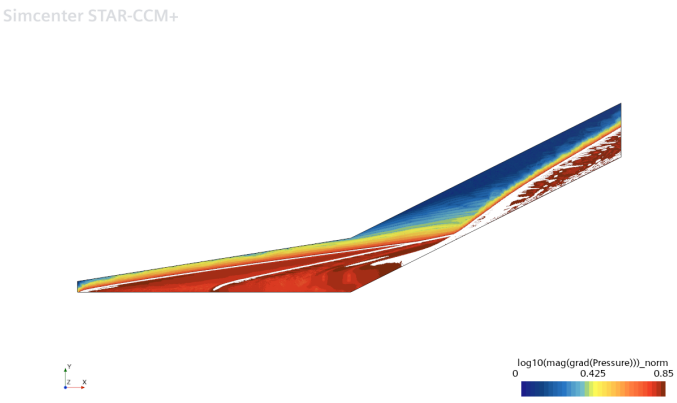

Figure 5.34: Pressure Gradient - Expansion - Boundary Layer Shocks Interaction

The expansion in this case is weak but the absolute pressure contours highlight the expansion which starts from the triple point and reflects to the wall.

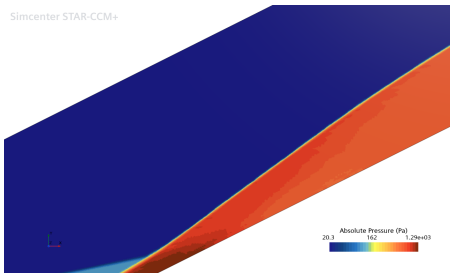

Figure 5.35: Absolute Pressure - Expansion - Boundary Layer Shocks Interaction

5.8.3 Slip Line Sensor

The slip line is detected with the following parameters:

- Normalized Density Gradient: ($> 87.5\%$)
- Normalized Pressure Gradient: ($< 90\%$)
- Normalized Mach Gradient: ($< 90\%$)

Density Gradient Condition

With respect to the inviscid case, the normalized density gradient condition is necessary to isolate the slip line with a better resolution and accuracy.

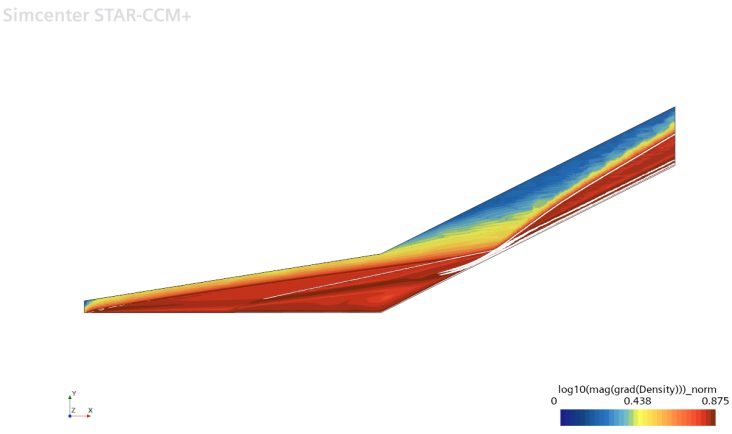

Figure 5.36: Density Gradient - Slip Line - Boundary Layer Shocks Interaction

Pressure Gradient Condition

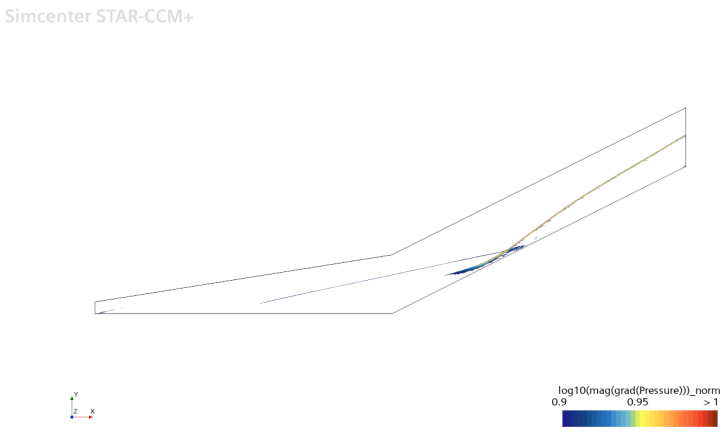

Figure 5.37: Pressure Gradient - Slip Line - Boundary Layer Shocks Interaction

Mach Gradient Condition

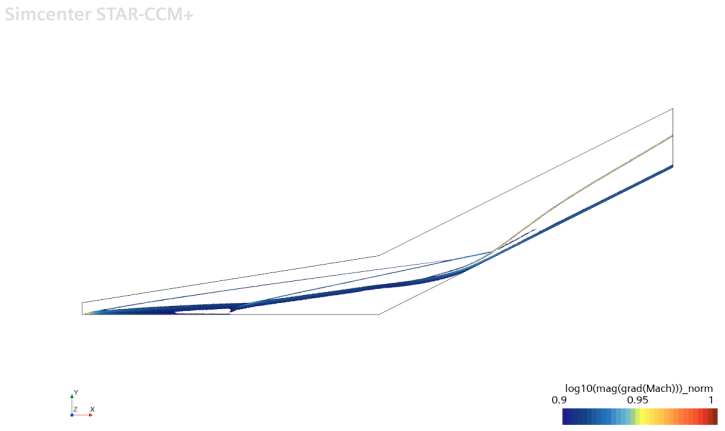

Figure 5.38: Mach Gradient - Slip Line - Boundary Layer Shocks Interaction

The combination of the conditions gives in output exactly the slip line without empty regions or numerical oscillations.

5.9 Wake

5.9.1 Shock Sensor

The shocks are detected with the following parameters:

- Mach normal: $(-3.5; -0.5)$
- Normalized Pressure Gradient: $(> 80\%)$

Mach Normal Condition

The Mach normal condition captures the bow shock and the reattachment shocks. The range used is more accurate and precise.

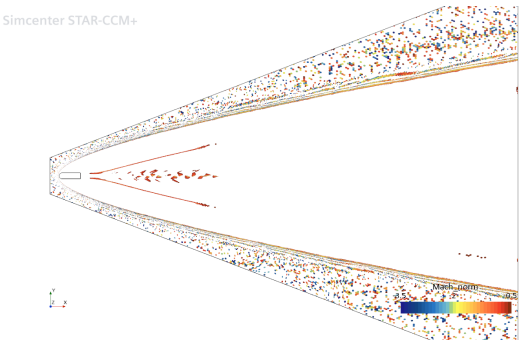

Figure 5.39: Mach Normal - Shock - Wake

Gradient Condition

The gradient condition isolates the shocks and the first part of the expansion in the nose region. The combination with the Mach normal condition captures exactly the shocks.

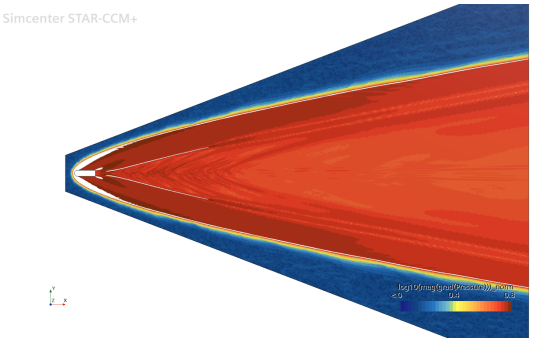

Figure 5.40: Pressure Gradient - Shock - Wake

5.9.2 Wake Sensor

The wake is detected with the following parameters:

- Total Temperature: ($< 90\%$)

Total Temperature Condition

As explained in the wake sensor definition, the normalized total temperature threshold is sufficient to capture the wake. The contours show the difference between the wake and the freestream. A cut below the 90 % captures exactly the wake where the total temperature changes, excluding the freestream with the maximum total temperature.

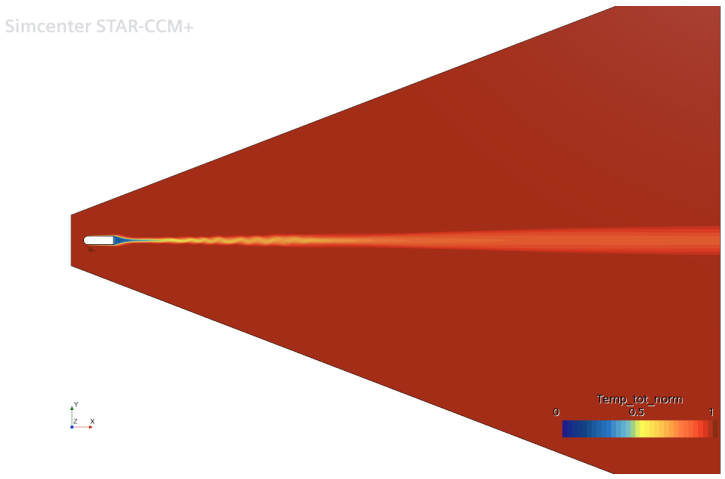

Figure 5.41: Total Temperature - Wake - Wake

5.9.3 Expansion Sensor

The expansion is detected with the following parameters:

- Mach normal: (0.5; 2.5)
- Normalized Pressure Gradient: ($> 78.5\%$)

The expansion parameters are proposed to complete the case. The pressure gradient is more sensible to capture the supersonic expansion and the Mach normal parameters are included in the standard range used in all the cases.

Chapter 6

Results

6.1 Ramp

6.1.1 Shock Sensor

The definitive shock sensor function for the ramp case is:

```
${Mach_norm}> -1.5 && ${Mach_norm}< -0.5 && ${log10(mag(grad(Pressure)))_norm} > 0.9 ? 1: 0
```

The combination of the two conditions gives in output exactly the shock wave, excluding the other flow features. The shock is captured with extreme precision as a sharp thin layer impinging on the corner. As expected from the theory, the oblique shock wave is generated by the impact with the left turning wall which turns the flow toward the flow itself.

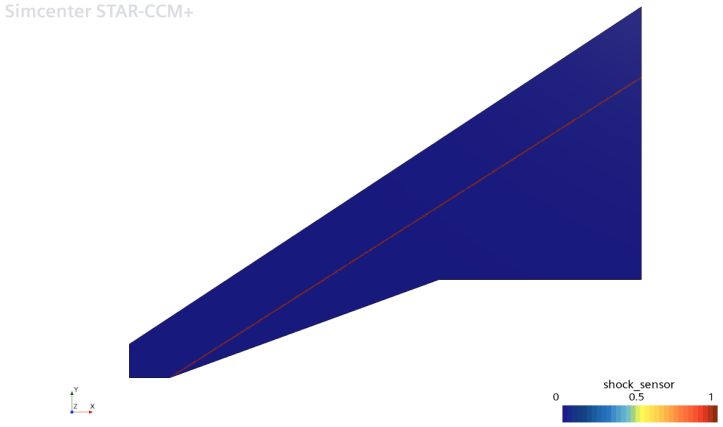

Figure 6.1: Shock Sensor - Ramp

6.1.2 Expansion Sensor

The definitive expansion sensor function for the ramp case is:

```
${Mach_norm}> 0.5 && ${Mach_norm}< 2 && ${log10(mag(grad(Mach)))_norm} > 0.75 ? 2: 0
```

The combination gives in output the expansion fan and some spurious gradients close to the shock wave.

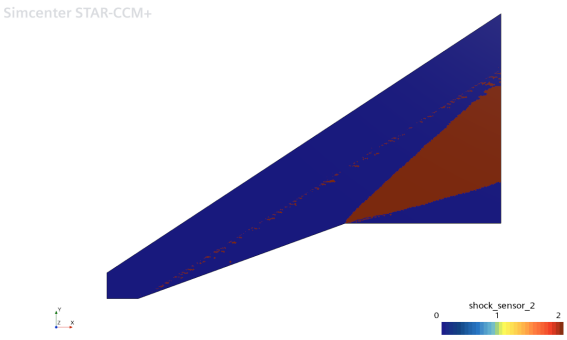

Figure 6.2: Expansion Sensor - Ramp

6.1.3 Smoothed Expansion Sensor

A filtering operation is necessary to smooth the detection. The expansion is well isolated with a 10 % threshold on the normalized absolute pressure. The expansion fan is thus detected smoothly as the classical Prandtl-Meyer expansion fan.

```
${Mach_norm}> 0.5 && ${Mach_norm}< 2 && ${log10(mag(grad(Mach)))_norm} > 0.75 && ${abs_Pressure_norm} < 0.9 ? 2: 0
```

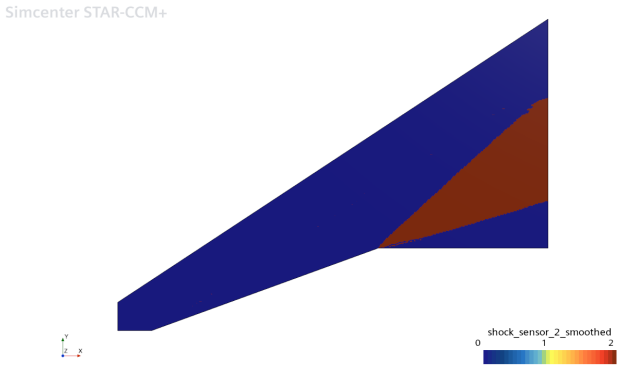

Figure 6.3: Smoothed Expansion Sensor - Ramp

6.1.4 Total Sensor

The sensors can be combined in a total sensor to have a complete visualization of the flow features desired with different colours. The shock sensor has index equal to 1 and expansion sensor has index equal to 2.

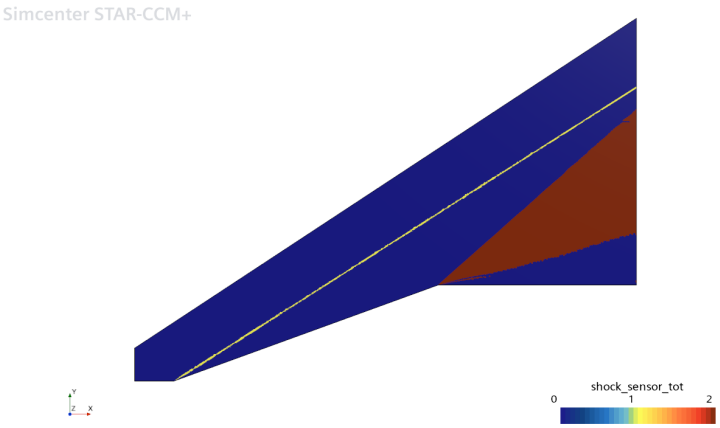

Figure 6.4: Total Sensor- Ramp

6.1.5 Mesh Refinement

The mesh refinement scene shows the different refinement level in the shock and expansion regions with respect to the freestream governed by the exponential.

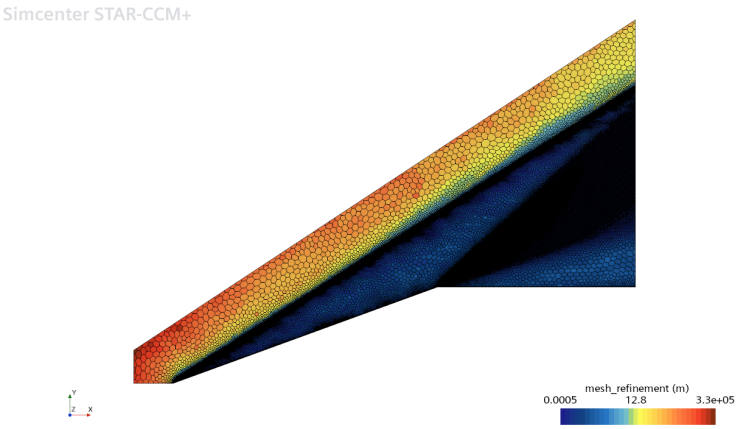

Figure 6.5: Mesh Refinement - Ramp

6.2 Blunt Body 1

6.2.1 Shock Sensor

The definitive shock sensor function for the inviscid blunt body case is:

```
${Mach_norm}> -3.5 && ${Mach_norm}< -0.5 && ${log10(mag(grad(Pressure)))_norm} > 0.925 ? 1: 0
```

The shock is greatly captured as a curve and detached shock wave. As expected from the theory, the critical slope of the wall causes the curve and detached shock with a large shear layer between the shock and the corner. The Mach normal range is larger with respect to the standard to have an accurate detection of the shock wave as a curve and thin wave.

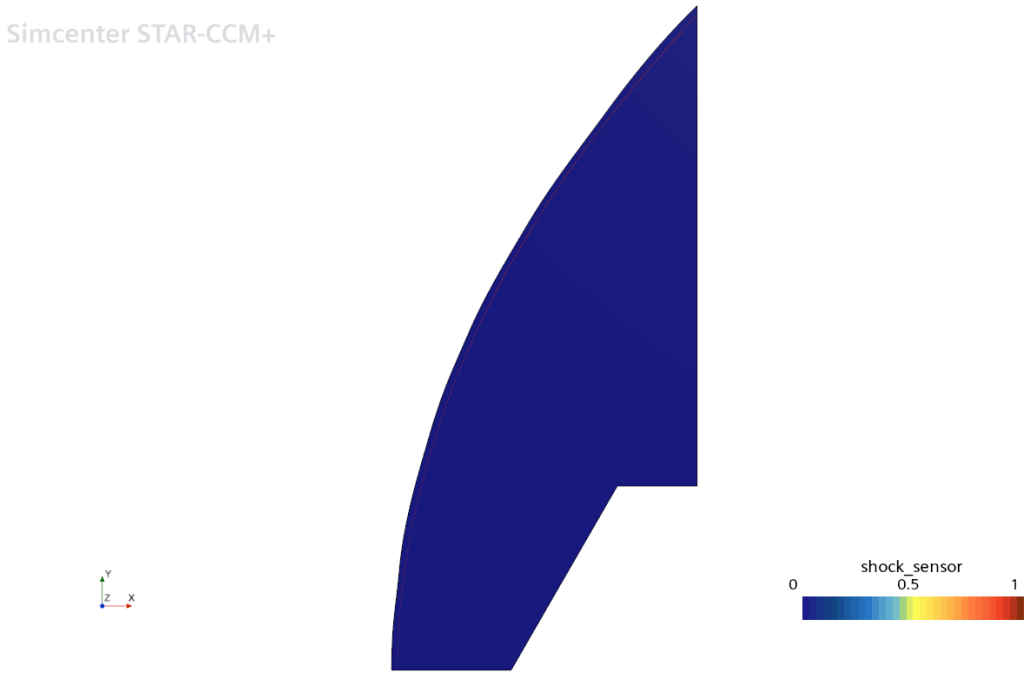

Figure 6.6: Shock Sensor - Blunt Body 1

6.2.2 Expansion Sensor

The definitive expansion sensor function for the blunt body case is:

```
${Mach_norm}> 0.5 && ${Mach_norm}< 2 && ${log10(mag(grad(Mach)))_norm} > 0.775 ? 2 : 0
```

The expansion is detected as a uniform region but is considerably different from the classic Prandtl-Meyer fan due to the strong irregularities in all the flow field.

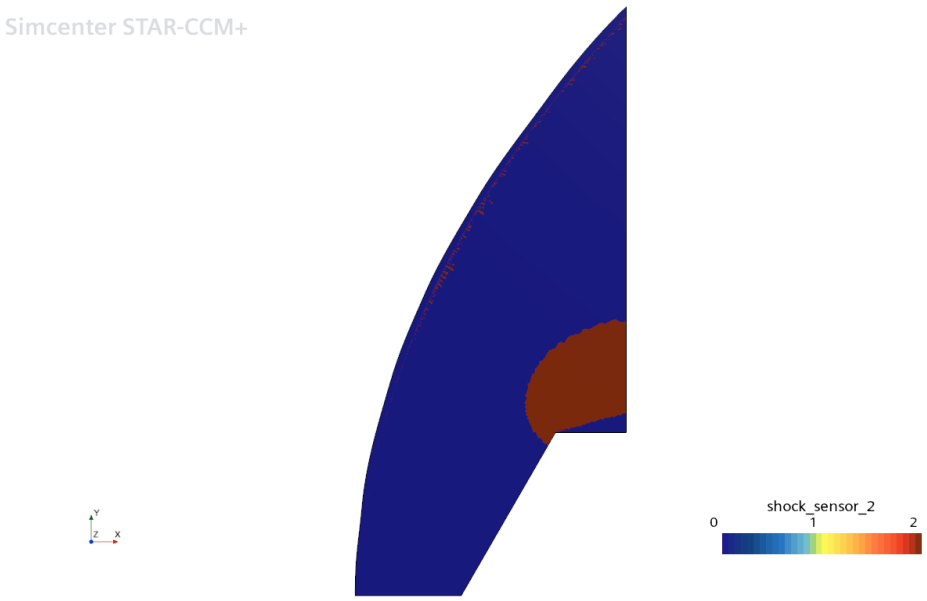

Figure 6.7: Expansion Sensor - Blunt Body 1

6.2.3 Smoothed Expansion Sensor

The expansion is isolated with a 55 % threshold on the normalized absolute pressure. However, the filtering operation not only removes the noises but smooths the expansion with a different shape leading to a non physical solution. Here is proposed the smoothed sensor definition only as a hint for future developments.

```
${Mach_norm}> 0.5 && ${Mach_norm}< 2 && ${log10(mag(grad(Mach)))_norm} > 0.775 &&  ${abs_Pressure_norm} < 0.45 ? 2 : 0
```

6.2.4 Total Sensor

The shock sensor has index equal to 1 and expansion sensor has index equal to 2.

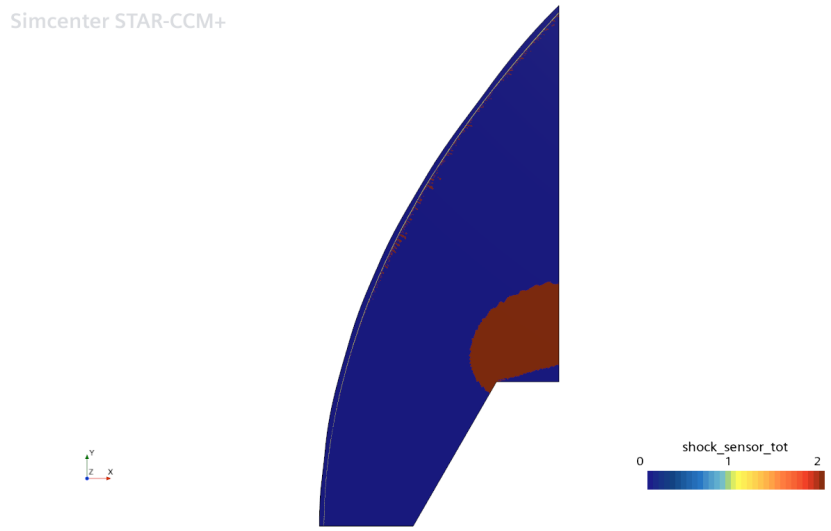

Figure 6.8: Total Sensor - Blunt Body 1

6.2.5 Mesh Refinement

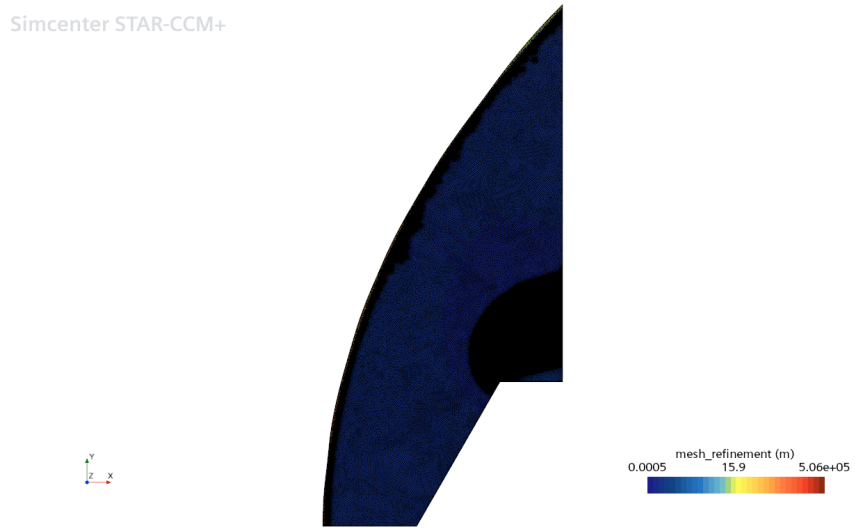

Figure 6.9: Mesh Refinement - Blunt Body 1

6.3 Shocks Interaction

6.3.1 Shock Sensor

The definitive shock sensor function for the shocks interaction case is:

```
${Mach_norm}> -1.5 && ${Mach_norm}< 0.5 && ${log10(mag(grad(Pressure)))_norm} > 0.925 ? 1 : 0
```

The two oblique shock waves and the coalescent shock are accurately detected. The 92.5 % is the precise rate to capture accurately the three shocks. The sensor clearly recognize the oblique shock waves generated by the impact with the two corner with different inclinations and the coalescent shock caused at the triple point.

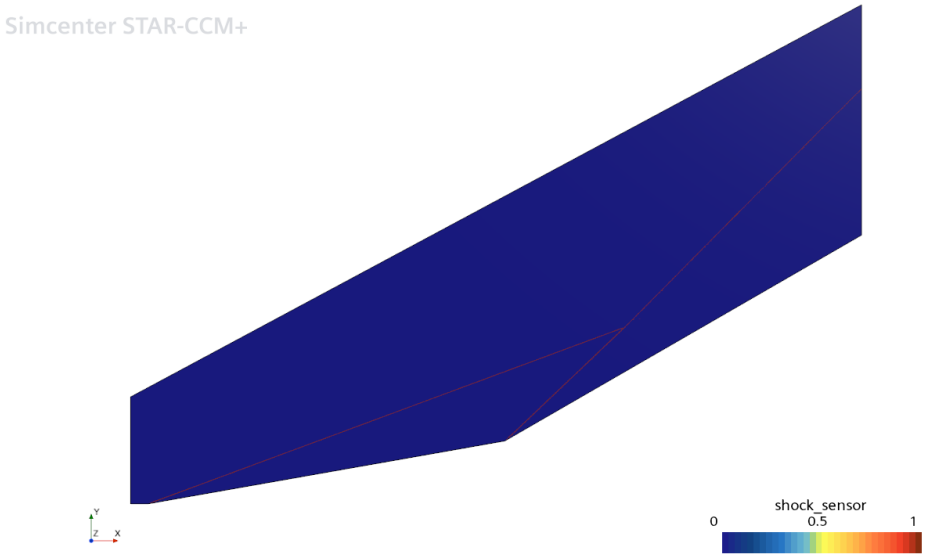

Figure 6.10: Shock Sensor - Shocks Interaction

6.3.2 Expansion Sensor

The definitive expansion sensor function for the shocks interaction case is:

```
${Mach_norm}> 0.5 && ${Mach_norm}< 2 && ${log10(mag(grad(Mach)))_norm} > 0.875 ? 3 : 0
```

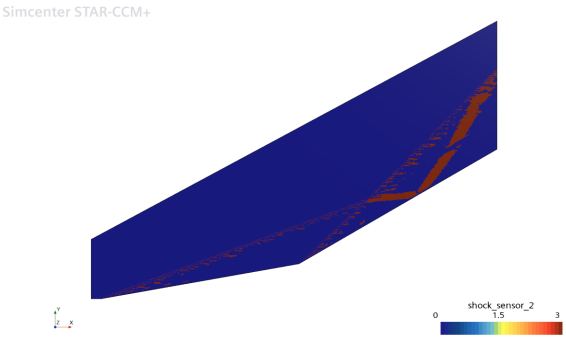

Figure 6.11: Expansion Sensor - Shocks Interaction

6.3.3 Smoothed Expansion Sensor

The detection is characterized by numerical impurities removed with a double threshold depending on the region: the first part is smoothed with a range between 75 % and 80 %, the second part, reflected by the wall, from 85 % to 90 %. The filtering operation not only removes the noises but smooths the expansion precisely.

```
${Mach_norm}> 0.5 && ${Mach_norm}< 2 && ${log10(mag(grad(Mach)))_norm} > 0.875 && ${abs_Pressure_norm} > 0.75 && ${abs_Pressure_norm} < 0.8 ? 3 : 0
${Mach_norm}> 0.5 && ${Mach_norm}< 2 && ${log10(mag(grad(Mach)))_norm} > 0.875 && ${abs_Pressure_norm} > 0.85 && ${abs_Pressure_norm} < 0.9 ? 3 : 0
```

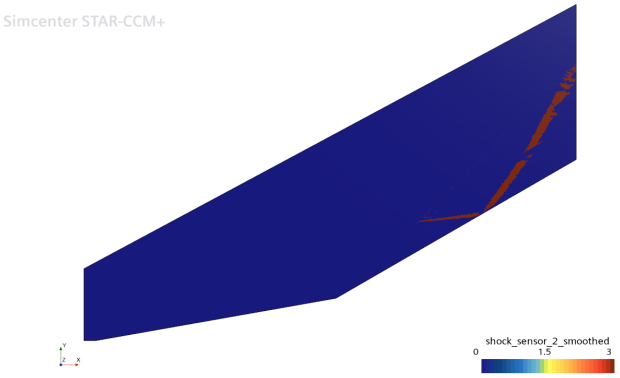

Figure 6.12: Smoothed Expansion Sensor - Shocks Interaction

6.3.4 Slip Line Sensor

The definitive slip line sensor function for the shocks interaction case is:

```
${log10(mag(grad(Pressure)))_norm} < 0.875 && ${log10(mag(grad(Mach)))_norm} > 0.945 ? 2 : 0
```

The slip line is perfectly detected through the combination of a relevant Mach gradient and a low pressure gradient. The parameters imposed are optimum, in fact changing also a small delta in the function could lead to detection errors.

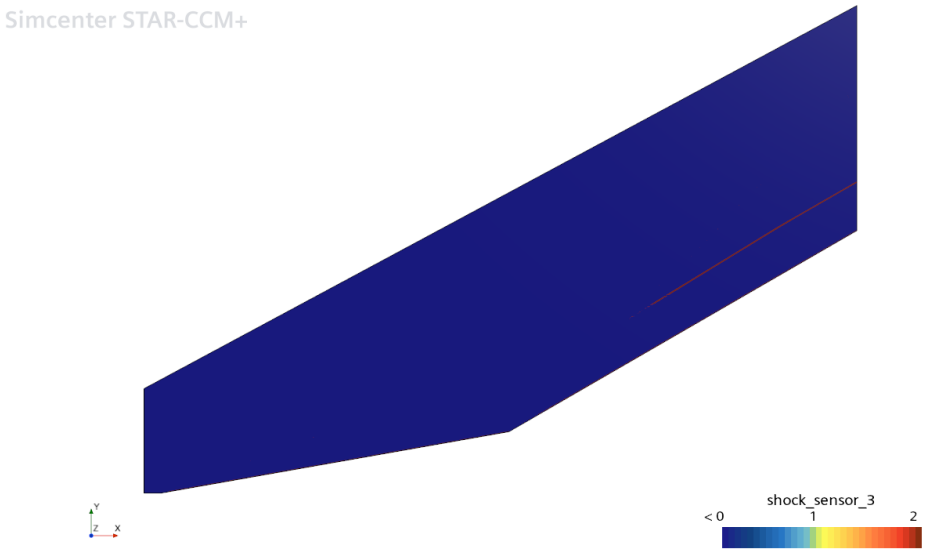

Figure 6.13: Slip Line Sensor - Shocks Interaction

6.3.5 Total Sensor

The shock sensor has index equal to 1, the expansion sensor has index 3 and the slip line sensor equal to 2. The index is assigned only in visualization terms.

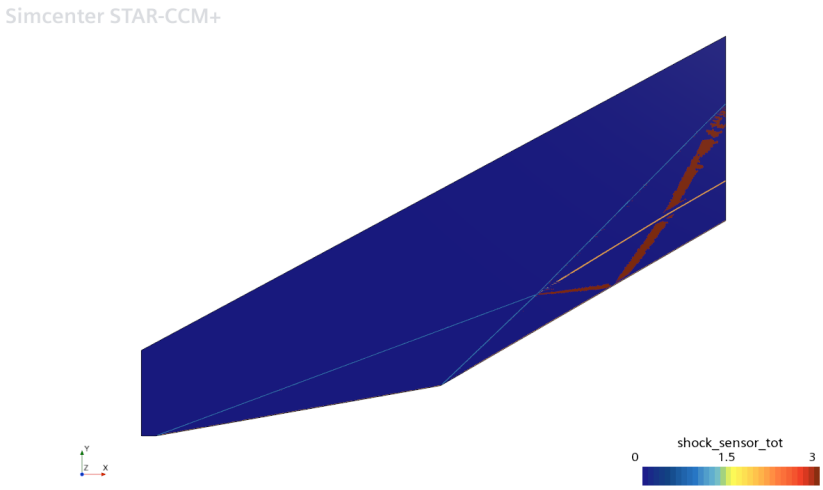

Figure 6.14: Total Sensor - Shocks Interaction

6.3.6 Mesh Refinement

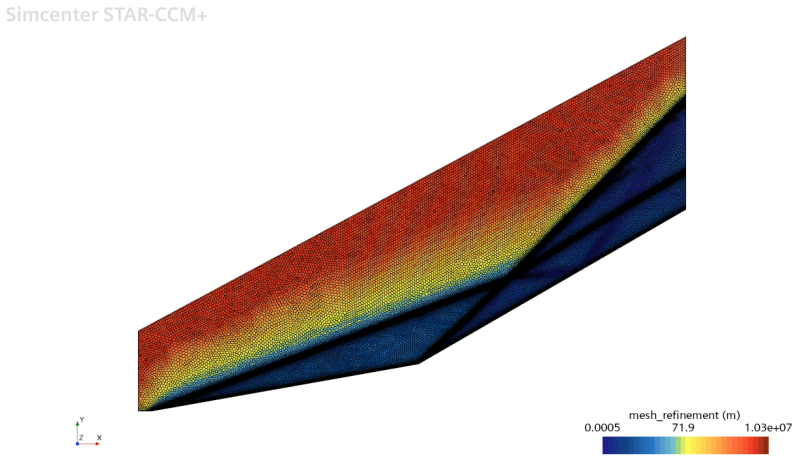

Figure 6.15: Mesh Refinement - Shocks Interaction

6.4 Flat Plate

6.4.1 Shock Sensor

The definitive shock sensor function for the flat plate case is:

```
${Mach_norm}> -1.5 && ${Mach_norm}< -0.5 && ${log10(mag(grad(Pressure)))_norm} > 0.9 ? 1: 0
```

The shock impinging on the boundary layer is accurately captured. The nose region is difficult to detect because is strongly characterized by the interaction of the freestream with the shock and the boundary layer. However the detection result is clear and the shock is shown as sharp thin layer.

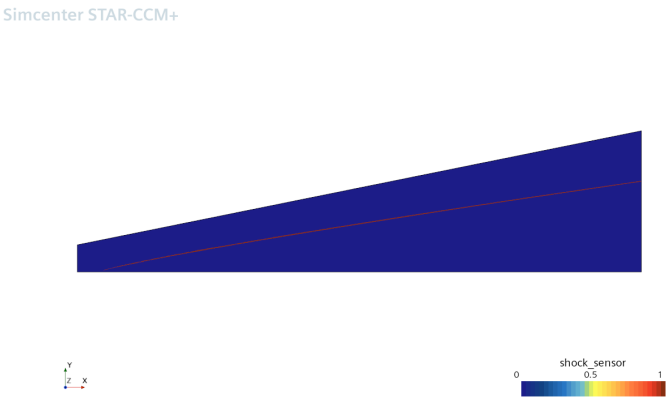

Figure 6.16: Shock Sensor - Flat Plate

6.4.2 Mesh Refinement

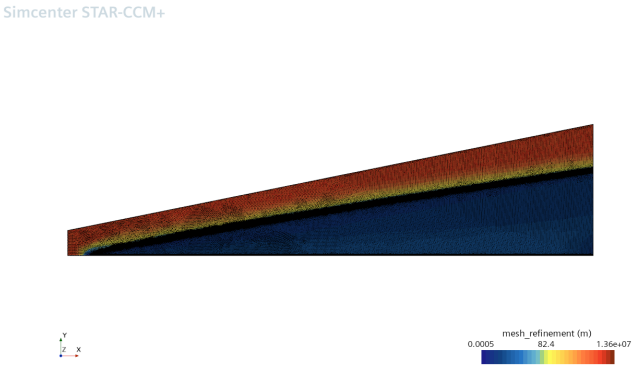

Figure 6.17: Mesh Refinement - Flat Plate

6.5 Blunt Body 2

6.5.1 Shock Sensor

The definitive shock sensor function for the viscous blunt body case is:

```
${Mach_norm}> -3.5 && ${Mach_norm}< -0.5 && ${log10(mag(grad(Pressure)))_norm} > 0.9 ? 1: 0
```

The shock is efficiently captured as a curve and detached shock. The parameters imposed for both the conditions are equal to the inviscid case, therefore the sensor works efficiently despite the presence of the boundary layer.

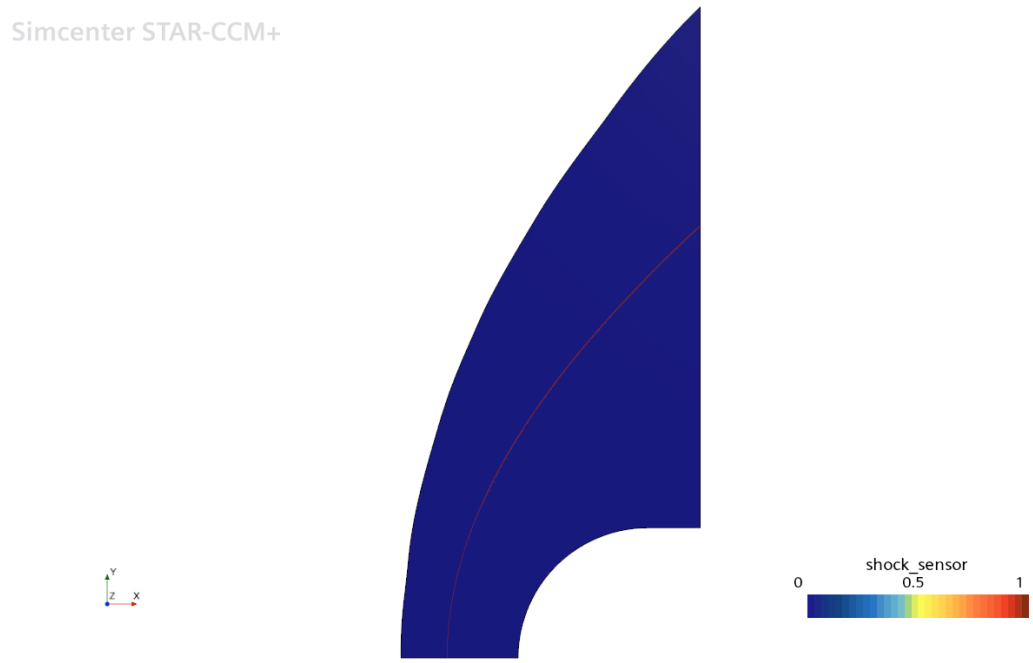

Figure 6.18: Shock Sensor - Blunt Body 2

6.5.2 Expansion Sensor

The definitive expansion sensor function for the viscous blunt body case is:

```
${Mach_norm}> 0.5 && ${Mach_norm}< 2 && ${log10(mag(grad(Pressure)))_norm} > 0.86 ? 2: 0
```

The expansion is detected as a uniform region but different from the classical Prandtl-Meyer fan. For this irregular case the pressure gradient substitutes the Mach gradient which is not that accurate to capture the expansion. Moreover, the gradient percentage is higher than the other cases due to the intensity of the expansion. The region close to the sonic line is characterized by strong perturbations and numerical impurities. This is the only case treated where the smoothing operation is insufficient. The condition imposed on the absolute pressure cuts the entropy gradients together with part of the expansion, influencing the physics of the problem.

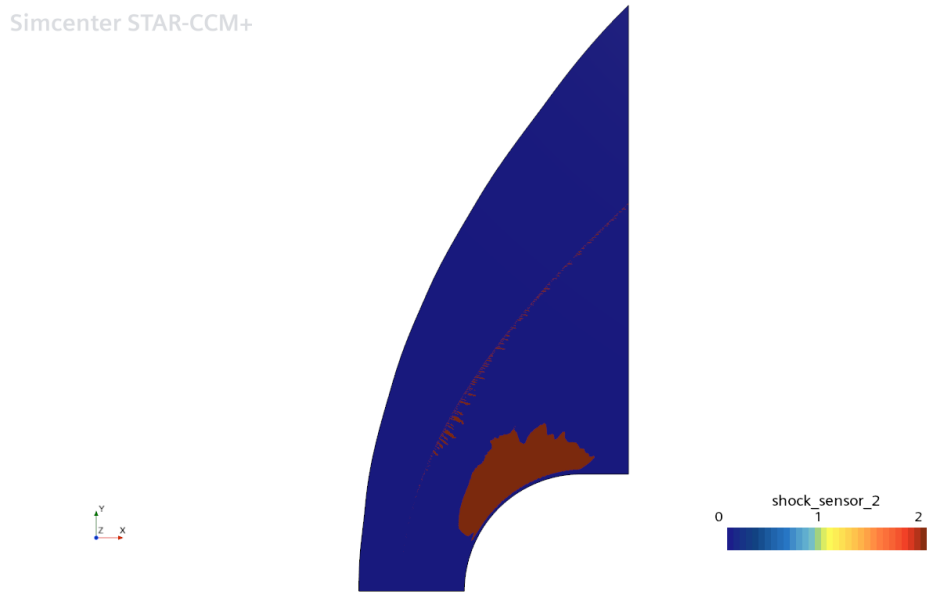

Figure 6.19: Expansion Sensor - Blunt Body 2

6.5.3 Total Sensor

The shock sensor has index equal to 1 and expansion sensor has index 2.

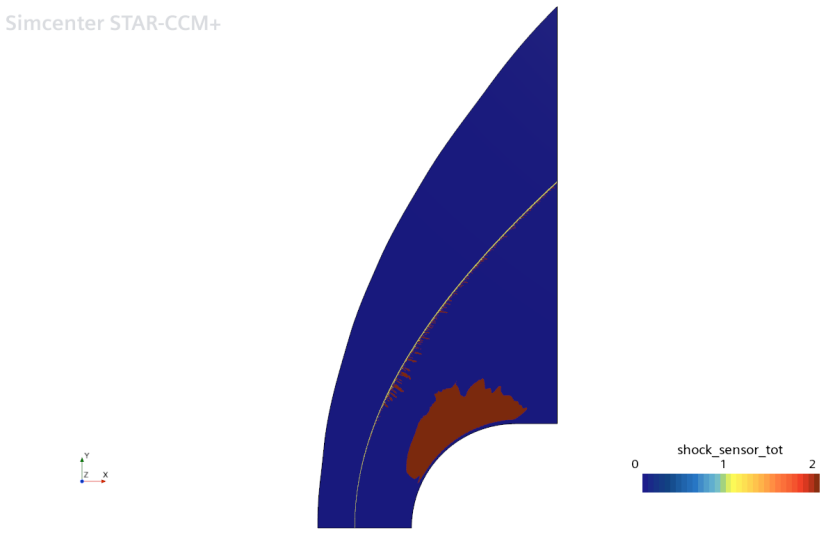

Figure 6.20: Total Sensor - Blunt Body 2

6.5.4 Mesh Refinement

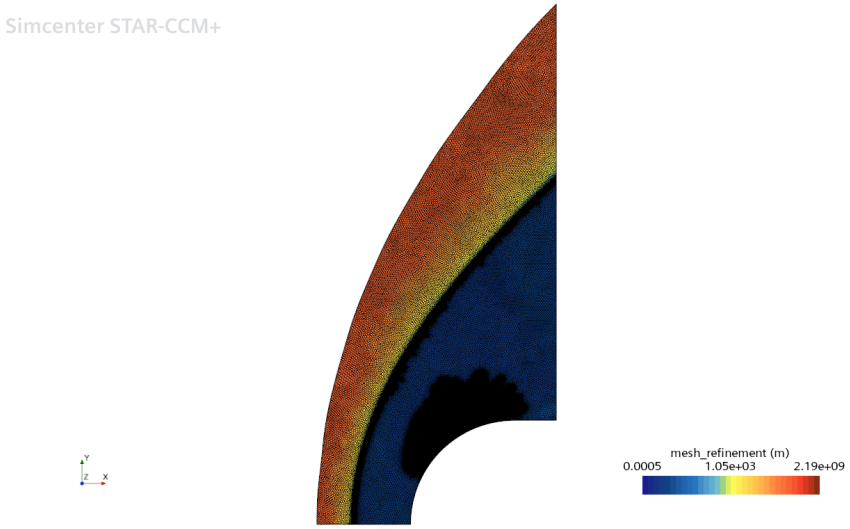

Figure 6.21: Mesh Refinement - Blunt Body 2

6.6 Boundary Layer Shocks Interaction

6.6.1 Shock Sensor

The definitive shock sensor function for the boundary layer interaction case is:

```
${Mach_norm}> -1.5 && ${Mach_norm}< -0.5 && ${log10(mag(grad(Pressure)))_norm} > 0.865 && ${abs_Pressure_norm} < 0.4 ? 1: 0
```

All the shock are detected with high accuracy. A filtering condition is applied to remove small impurities due to the coalescent shock in the interaction region. The shocks detection result highlights with precision the shock impinging on the corner, the shock generated by the impact on the separation bubble, the inner and outer shocks produced by the flow reattachment and the two final coalescent shocks.

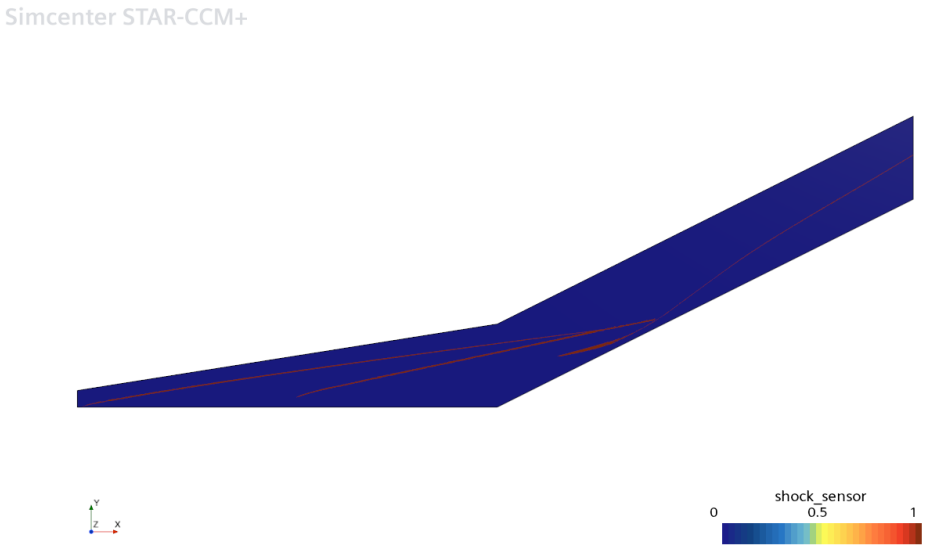

Figure 6.22: Shock Sensor - Boundary Layer Shocks Interaction

6.6.2 Expansion Sensor

The definitive expansion sensor function for the boundary layer interaction case is:

```
${Mach_norm}> 0.5 && ${Mach_norm}< 2.5 && ${log10(mag(grad(Pressure)))_norm} > 0.85 && ${abs_Pressure_norm} > 0.5 ? 2 : 0
```

In this case the expansion is weak given the interaction with the multiple shocks and the slip line. Therefore, the sensor detects a poor region exactly starting from the intersection point and slightly reflecting to the wall. In fact, the sensor includes the filtering condition which not only removes some numerical impurities but isolates better the expansion with a 50 % threshold. Also in this case, the pressure gradient is more sensible to the expansion detection and the rate equal to 85 % perfectly captures the feature. A different percentage could introduce errors in the detection.

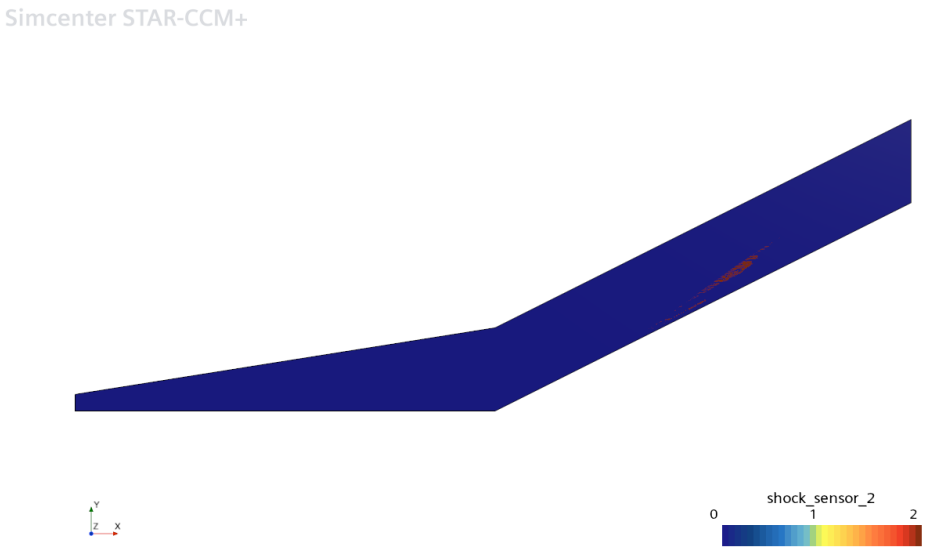

Figure 6.23: Expansion Sensor - Boundary Layer Shocks Interaction

6.6.3 Slip Line Sensor

The definitive slip line sensor function for the boundary layer interaction case is:

```
${log10(mag(grad(Density)))_norm} > 0.875 && ${log10(mag(grad(Mach)))_norm} < 0.905 && ${log10(mag(grad(Pressure)))_norm} < 0.895  &&  ${temp_tot_norm} > 0.99 ? 3 : 0
```

The condition about the density discontinuity is necessary to detect the slip line in this complex case. The standard condition about Mach and pressure gradient is not sufficient to the detection. Without the density condition the solution presents empty regions along the slip line. The thresholding condition about the total temperature excludes the boundary layer in the detection. In this way the slip line is not affected by the interaction with the bubble reattachment with the edge. The sensor is very sensible and the slip line is captured with extreme accuracy and precision. A different percentage could introduce errors in the detection.

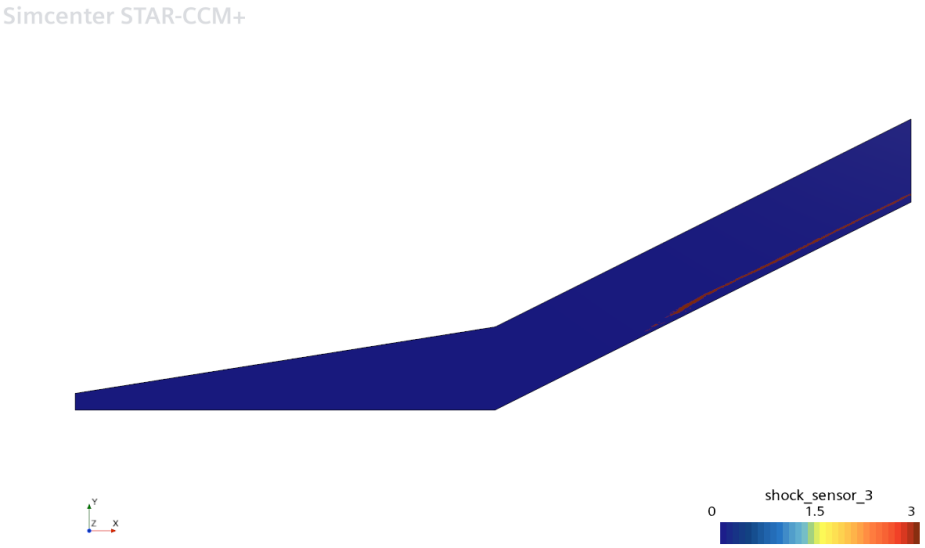

Figure 6.24: Slip Line Sensor - Boundary Layer Shocks Interaction

6.6.4 Total Sensor

The shock sensor has index equal to 1, the expansion sensor has index equal to 2 and the slip line sensor equal to 3.

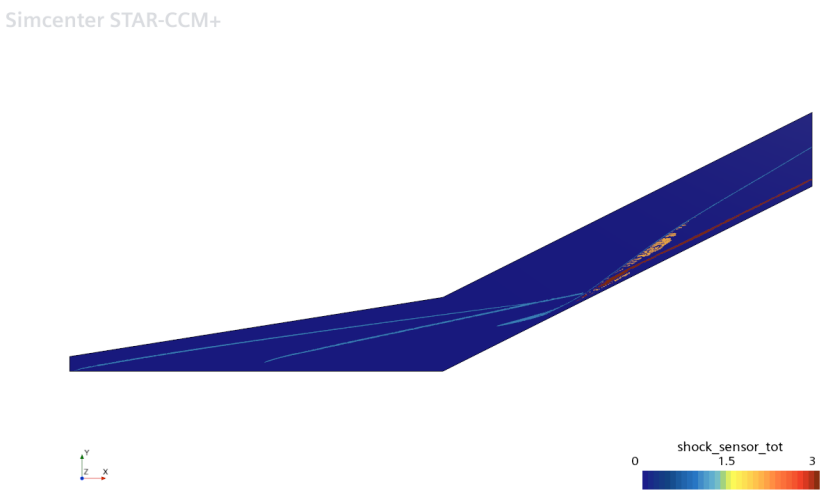

Figure 6.25: Total Sensor - Boundary Layer Shocks Interaction

6.6.5 Mesh Refinement

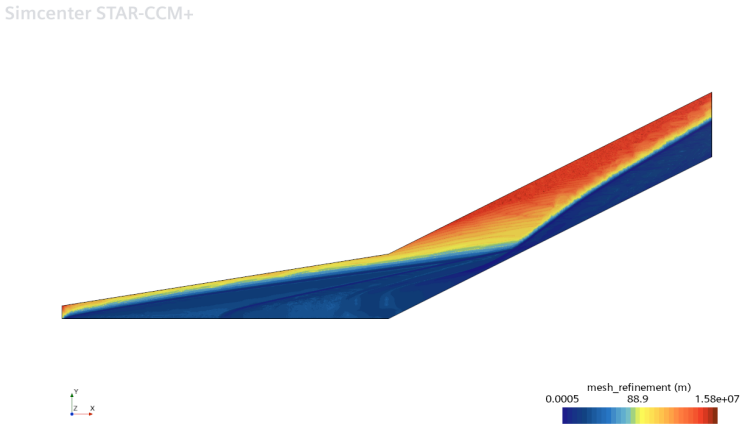

Figure 6.26: Mesh Refinement - Boundary Layer Shocks Interaction

6.7 Wake

6.7.1 Shock Sensor

The definitive shock sensor function for wake case is:

```
${Mach_norm}> -3.5 && ${Mach_norm}< -0.5 && ${log10(mag(grad(Pressure)))_norm} > 0.8 ? 1: 0
```

The 80 % rate used for the gradient condition is necessary to capture both the bow shock and the reattachment shocks. An higher percentage would detect the strongest part of the shocks with empty spaces moving downstream in the flow field. Therefore, the parameters considered also for the Mach normal condition are perfect to detect smoothly the targeted flow features. The reattachment shocks does not continue to the end of the domain as the bow shock due to the fact that the streamlines are deflected by the expansions in that region. Moreover, when the bow shock becomes less intense the streamlines do not require the deflection of the expansion to be aligned with the freestream direction.

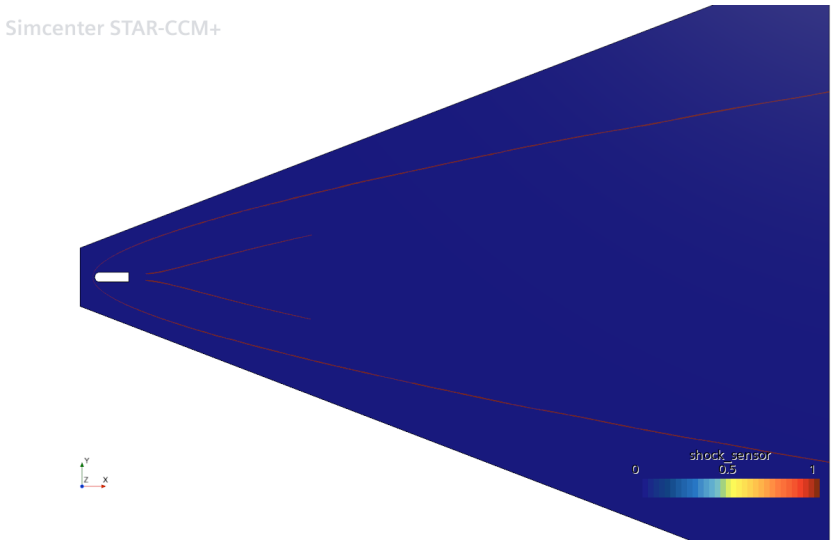

Figure 6.27: Shock Sensor - Wake

6.7.2 Expansion Sensor

The definitive expansion sensor function for the wake case is:

```
${Mach_norm}> 0.5 && ${Mach_norm}< 2.5 && ${log10(mag(grad(Pressure)))_norm} > 0.785 ? 3: 0
```

The expansion is well detected in the nose region. The expansion are also present in the region behind the body, where the turning geometry produces an increase in the velocity. However, the expansions continue moving downstream and the sensor is not that sensible to capture the complete feature without strong perturbations and entropy gradients. Plausible improvements, in fact, can regard the mesh refinement based also on the expansion to refine gradually the field and capture the final part. The total mesh refinement is not implemented given the long simulation time.

6.7.3 Wake Sensor

The definitive wake sensor function for the wake case is:

```
${Temp_tot_norm} < 0.9 ? 2 : 0
```

The wake is smoothly captured until the end of the fluid domain.

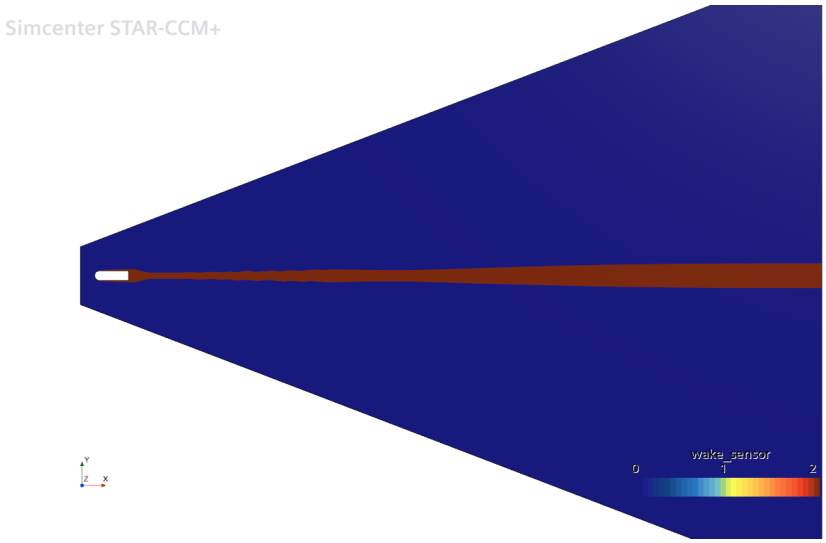

Figure 6.28: Wake Sensor - Wake

6.7.4 Total Sensor

The total sensor includes the shocks and wake sensors, as clearly shown.

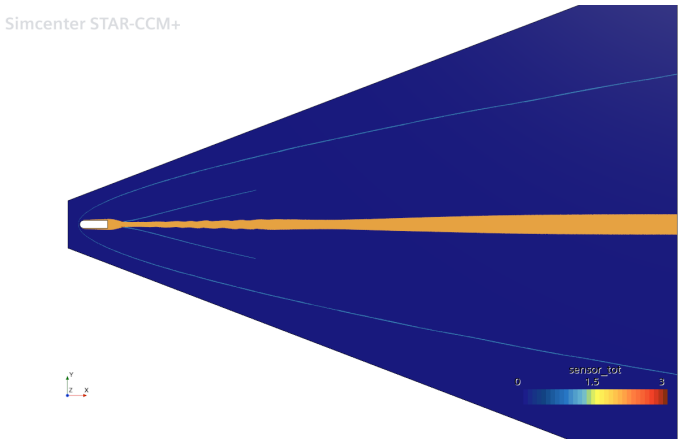

Figure 6.29: Total Sensor - Wake

6.7.5 Mesh Refinement

The mesh refinement is set in order to refine the flow field in the shocks and wake region indicated by the related sensors. Further improvements in the mesh refinement of this case can include the expansion sensor in the function and complete the refinement. The expansion sensor is now excluded given the heavy calculation time and mesh generation.

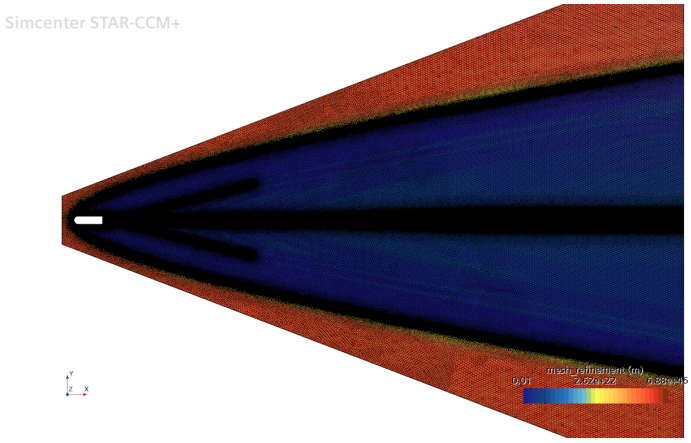

Figure 6.30: Mesh Refinement - Wake

6.8 Proposed Parameters

At the end of the work a summary shows the parameters considered for the detection and the related application range. The purpose is to test the sensors to obtain a universal formulation suitable for each case. In this way, the user can execute the detection in a general problem just using the parameters proposed. The shock and expansion sensors are compared for each case treated and the slip line sensor is tested and compared for the Edney cases. In this section is not proposed a summary about the wake sensor given the fact that it has been tested only on one model. Future improvements, in fact, concern the wake sensor test on other cases.

6.8.1 Shock Sensor

In the table is shown a summary of the shock detection parameters related to the two conditions about the Mach normal and the normalized pressure gradient for each test case. Generally, the shock is well detected in the 10 % highest gradients. However, the range proposed are the exact values imposed to obtain the better resolution and accuracy in the contours. Therefore, the proposed parameter for the shock detection are proposed in the following tables.

Case	M_n [/]	∇p_{norm} [%]
Ramp	(-1.5; -0.5)	0.9
Blunt 1	(-3.5; -0.5)	0.925
Shocks Int	(-1.5; -0.5)	0.925
Flat Plate	(-1.5; -0.5)	0.9
Blunt 2	(-3.5; -0.5)	0.9
Bl Shocks Int	(-1.5; -0.5)	0.865

Table 6.1: Parameters Summary - Shock Sensor

M_n [/]	∇p_{norm} [%]
(-1.5; -0.5)	(0.85 - 0.95)

Table 6.2: Proposed Parameters - Shock Sensor

The Mach normal condition works efficiently in the range (-1.5; -0.5), but in the complex case of bow shock the range (-3.5; -0.5) captures better the shock. To summarize, the shock is always well detected in the 15 % highest pressure gradients with the transition from -1.5 to -0.5 about the Mach normal.

6.8.2 Expansion Sensor

In the table is shown a summary of the expansion detection parameters related to the two conditions about the Mach normal and the normalized Mach gradient for each test case. The expansion is well detected in the 25 % highest gradients.

Case	M_n [/]	∇M_{norm} [%]
Ramp	(0.5; 2)	0.75
Blunt 1	(0.5; 2)	0.775
Shocks Int	(0.5; 2)	0.875
Blunt 2	(0.5; 2)	0.86*
Bl Shocks Int	(0.5; 2)	0.85*

Table 6.3: Parameters Summary - Expansion Sensor

M_n [/]	∇M_{norm} [%]
(0.5; 2)	(0.75 - 0.85)

Table 6.4: Proposed Parameters - Expansion Sensor

To summarize, the expansion is always well detected in the 25 % highest Mach gradients with the transition from 0.5 to 2 about the Mach normal. In the complex cases (*), the pressure gradient is more sensible to the flow discontinuities and a lower range of gradients, equal to 15 %, is sufficient to catch the expansion.

6.8.3 Slip Line Sensor

The slip line sensor is a particular case given the complex nature of the related flow feature. In fact, it is not possible to extract definitive parameters as for the other sensors. For the shocks - boundary layer interaction case it is necessary also the condition about the density gradient and the total temperature to make the sensor stronger given the boundary later interference. Moreover, the values used for the detection are the exact parameters to catch the slip line with the better resolution and without empty spaces in the results.

Case	∇M_{norm} [/]	∇p_{norm} [%]	$\nabla \rho_{norm}$ [%]
Shocks Int	0.945	0.875	-
Bl Shocks Int	0.9	0.9	0.875

Table 6.5: Parameters Summary - Slip Line Sensor

Chapter 7

Conclusions

To conclude, a final section summarizes the work about the objectives achieved. The purpose of the work is to drive the mesh refinement through the sensors created for the detection of shock, expansion waves, slip lines and wakes. Starting from the mesh refinement, different ways to refine the grid has been adopted. The definitive refinement function is defined in order to refine the regions indicated by the sensors with a cell's size chosen by the user and the remaining flow field gradually through the exponential function based on the gradient. Therefore, the sensors help the refinement function to speed up the process and thus reduce the number of mesh generation. In fact, a sensor based function needs less than half number of mesh generation with respect to the first mesh refinement function based directly on the gradient. Moving to the complementary phase of sensors creation, a quick summary about all the case studies is here proposed. The shock wave are always well detected both for the ramp type and the blunt body cases. The expansion is the most particular feature and is not always detected as the classical Prandtl-Meyer, especially for the blunt body and Edney cases where the strong entropy gradients affect the solution. The slip line requires severe conditions and is highly problem dependent. However, the definition proposed in the work is optimum to capture the feature with high accuracy and precision. The wake sensor does not require the logarithmic value of the variable and no gradient conditions are applied. In conclusion, the sensors created not only reflect the results expected from the theory but also are crucial to drive the refinement reducing strongly the simulation time. At the end of the work are presented the final detection parameters. In this way the user can choose a value in the range proposed to isolate the targeted fluid feature and create the related refinement function. This new method of detection entirely executed on the commercial software STAR-CCM+ is an innovative instrument to drive the grid refinement for various CFD high-speed applications.

Further analysis can regard the test on 3D simulations. The sensors can be applied to the 3D version of the cases considered to have a global visualization of the flow fields. In fact STAR-CCM+ allows to apply the Adaptive Mesh model to a 3D case and then set the conditions to operate the refinement according to the related procedure. In this way it could be possible to execute sensitivity analysis between the two mesh refinement methods and verify the accuracy of the sensors. Other future improvements concern the application of a filter, as the most common Gauss filter, through a post-processing operation. As mentioned, STAR-CCM+ does not allow to apply properly the Gauss circular mask in every point of the domain. The filtering operation applied is based on a combination of a smoothing and a physical condition based on the absolute pressure and it could be interesting to apply the Gauss circular mask on an more proper post-processing software. Lastly, various sensitivity analysis could be conducted to improve the mesh refinement function. For example the user can choose a different function to refine the flow field or a different geometric progression of the exponential function imposed. Moving on the sensors definition, another analysis can be conducted substituting the Mach with the pressure in the Mach normal condition. The two variable are quite similar but a detailed analysis can be useful to define precisely which condition is the most accurate for the detection. In conclusion, the sensors are deeply tested to various case studies and the mentioned analysis could be executed to complete the work.

Bibliography

[1] Anderson J.D. Jr. *Hypersonic and High-Temperature Gas Dynamics*. Third Edition. AIAA, 2019. DOI: 10.2514/4.105142.

[2] Canny J.F. «A computational approach to edge detection». In: *IEEE Transactions on Pattern Analysis and Machine Intelligence* (Dec. 1986), pp. 679–698.

[3] Fujimoto T.R., Kawasaki T., and Kitamura K. «Canny-Edge-Detection/ Rankine-Hugoniot-conditions unified shock sensor for inviscid and viscous flows». In: *Journal of Computational Physics* (July 2019), pp. 264–279.

[4] Sabetta F. *Corso di Gasdinamica - Capitolo 5 - Flussi piani supersonici con onde d'urto*. 2010. URL: http://dma.ing.uniroma1.it/users/ls_gas/MATERIALE/cap5.pdf.

[5] Anderson J.D. Jr. *Fundamentals of Aerodynamics 6th Edition*. 6^{th} Edition. McGraw Hill, 2016.

[6] F Ducros et al. «Large-eddy simulation of the shock turbulence interaction». In: *Journal of Computational Physics* 152 (1999), pp. 517–549.

[7] E. Garnier, P. Sagaut, and M. Deville. «A class of explicit ENO filters with application to unsteady flows». In: *Journal of Computational Physics* 170 (2001), pp. 184–204.

[8] S. Pirozolli. «Numerical methods for high-speed flows». In: *Annu. Rev. Fluid Mech.* 43 (2011), pp. 163–194.

[9] M. Kanamori and K. Suzuki. «Shock wave detection in two-dimensional flow based on the theory of characteristics from CFD data». In: *Journal of Computational Physics* (2011), pp. 3085–3092.

[10] T.J. Barth. «Some Notes on Shock-Resolving Flux Functions». In: *Part 1: Stationary Characteristics, Ames Research Center* (1989), p. 101087.

[11] Ziniu Wu, Yizhe Xu, Wenbin Wang, and Ruifeng Hu. «Review of shock wave detection method in CFD post-processing». In: *Chinese Journal of Aeronautics* 26.3 (2013), pp. 501–513. ISSN: 1000-9361.

[12] Pagendarm H.G. and Seitz B. «An algorithm for detection and visualization of discontinuities in scientific data fields applied to flow data with shock waves». In: *Palamidese P, editor. Scientific visualization: advanced software techniques. Delhi: Prentice Hall* (1993).

[13] Basu M. «Gaussian-based edge-detection methods-a survey». In: *IEEE Transactions on Systems, Man, and Cybernetics, Part C 32.3* (2002), pp. 252–260.

[14] Davies E. *Machine vision: Theory, Algorithms and Practicalities*. Amsterdam: Elsevier, 2008.

[15] «Siemens Digital Industries Software». In: *Simcenter STAR-CCM+ User Guide 2310.0001 (18.06.007-R8)* ().

[16] «Simcenter STAR-CCM+ Tutorial in Practice: Adaptive Mesh Refinement, YouTube, 12 Aug. 2021». In: ().

[17] «Simcenter STAR-CCM+ model-driven adaptive mesh refinement (AMR)». In: (2020).

[18] James G. Coder et al. «Output-based mesh adaptation for high-speed flows». In: *Computers and Fluids* 273 (2024), p. 106208.

[19] *Example : Adaptive Mesh Refinement on JCM Missile at Supersonic flow condition*. Siemens - Digital Industries Software. 2020. URL: `https://support.sw.siemens.com/it-IT/knowledge-base/KB000035722_EN_US`.

[20] Ahmed Shihab Ahmed. «Comparative Study Among Sobel, Prewitt and Canny Edge Detection Operators Used in Image Processing». In: *Journal of Theoretical and Applied Information Technology* Vol.96. No 19 (2018).

[21] Vincent. O. R. and Folorunso. O. «A Descriptive Algorithm for Sobel Image Edge Detection». In: *Proceedings of Informing Science IT Education Conference (InSITE)* (2009).

[22] Adlakha. D. Adlakha. D. and Tanwar. R. «Analytical Comparison between Sobel and Prewitt Edge Detection Techniques». In: *International Journal of Scientific Engineering Research* Vol.7 (Jan. 2016).

[23] Keiichi Kitamura, Philip Roe, and Farzad Ismail. «Evaluation of Euler Fluxes for Hypersonic Flow Computations». In: *AIAA JOURNAL* 47 (Jan. 2009).

[24] Lovely D. and Haimes R. «Shock detection from computational fluid dynamics results». In: *AIAA* (1999), pp. 99–3285.